ROYAL INSTITUTE
OF TECHNOLOGY

Stretched Pulse Generation in Erbium-doped Fibre Ring Laser

Master of Science Thesis

Mikael Tiihonen

Stockholm, January 2002

Supervisor: Dr Derryck T. Reid, Heriot-Watt University, Scotland.
Examiner: Professor Fredrik Laurell, Royal Institute of Technology, Sweden.

TRITA-FYS 2002:2
ISSN 0280-316X
ISRN KTH/FYS/--02:2—SE

Abstract

In this Master of Science thesis, I will discuss the construction of an Erbium-doped fibre ring-laser that emits in the spectral range of 1530 nm. Experimentally, two set-ups have been investigated and are briefly compared, i.e., forward and backward propagation of the laser beam in the ring. Both theoretical and experimental work has been carried out in this project. In the thesis, I give an overview of fibre ring-lasers and their characteristics. The work has included measurements of the group-velocity dispersion and numerical calculations of the non-linear Schrödinger equation. Key parameters (i.e., gain coefficient, dispersion, etc.) were varied in order to observe the differences in the operation of such lasers. During the time of this relatively brief project, no stable pulse operation could be obtained from the present set-ups. However, from the experimental know-how obtained during the project period and the numerical calculations carried out, this negative result can be explained.

Acknowledgement

First of all I would like to acknowledge my supervisor Professor Fredrik Laurell, for giving me the opportunity to pursue my Master project at Heriot-Watt University, Scotland. There Dr. Derryck Reid welcomed me in to his “ultra fast” group. From him I learned almost everything I know about constructing fibre lasers and lasers in general. I am very grateful for all the time he spent in the lab instructing me and always being around when I needed any help.

To my office-mates in G.04, David Artigas and Stephen Spears, thanks for interesting discussions in all fields, including physics. I will always be indebted to David for all the help in the art of numerical methods and physics that you so well understand. Thanks for all the great times we had in el Barrio (salsa!), the Highlands and Glasgow. You where always around when I needed anything: somewhere to stay, good coffee, money, Spanish lessons...

To the other members in the Ultra Fast Optics Group, Iain Cormack, Karl Tillman, Euan Ramsay and Heather, I wish you all good luck in the future and I hope we soon meet again.

I would like to express my thanks to all in the Fibre Group at Heriot-Watt for letting me handle their expensive equipment and assisting me with their fibre-knowledge. Especially, Gordon Flockhart for his patience when explaining DFTS, Robert Maier for interesting discussions late at night in their lab and Matthew Gander for the vacuum.

I would also like to thank Marconi Caswell Ltd for supplying pump laser diodes, Fibre Core Ltd for the erbium-doped fibre and Nortel for the pump diode that I broke.

I’m very grateful for all the friends that came over and visited me during this time, Niklas Österström, Johan Stenbäck, Caroline & Jenny, Jonas Hellström (d.y.) and above all Anna Möller.

To my grandparents I will always be in debt, without them I would not have reached this far, thank You.

Introduction

Passive mode locking is a powerful technique for ultrashort pulse generation in dye and solid-state lasers. One of the first techniques for passive mode locking was to use a dye saturable absorber, where the peak intensity and saturable absorber action increases as the pulse is shortened. In comparison, active mode locking is extremely sensitive to the imposed modulation frequency (that is usually driven with an externally electronic circuit) and the intermode frequency interval of the cavity ($c/2L_{cavity}$) and therefore makes it very difficult to establish subpicosecond regimes with just a single active locking procedure. The modulator response speed is limited by the driving electronics and is independent of the pulse duration. New techniques for passive mode locking have been developed, such as self-mode locking, discovered in 1991 by Sibbett et al. [1], also referred to as Kerr lens mode locking (KLM) and interferometric or additive pulse mode locking (APM). Mollenauer and Stolen first used the APM mechanism in a soliton laser in 1984, [2]. KLM and APM rely on the intensity dependent non-linear refractive index properties ($n = n_0 + n_2|E|^2$) of the crystals or fibres used, to achieve a saturable-absorber-like action. These new techniques laid the ground for developing a versatile third generation femtosecond laser technology with broadly tunable solid-state laser materials.
In contrast to mode locking with saturable absorbers based on dyes/semiconductors, APM and KLM do not rely on population excitation and thus can simulate an extremely fast and broadband saturable absorber action. Saturable absorber dyes have some drawbacks such as high insertion loss and a slow recovery time and, as a consequence their use has been limited for femtosecond generation.

KLM achieves fast saturable absorber action using self-focusing; this is due to the non-linear refractive index n_2. The Gaussian wave does not feel a homogeneous refractive index as it passes through the medium. The refraction is stronger on the axis of the beam than away from it, as a consequence the medium acts like a converging lens and focuses the beam just like a lens (Kerr lens). The Kerr lens effect has been known for a long time in non-linear optics, but was first used for mode locking in 1991 by Sibbett et al. in a Ti:sapphire laser. By adjusting the position of the crystal and using the focusing mirrors in the cavity, the Kerr effect causes the most intense parts of the wave to experience lower losses, which manifests itself as a stable condition for the cavity. The lower intensities are suppressed because these are subject to higher losses than the more intense part. Thus, KLM plays a part similar to that of saturable absorber in the passive mode locking method and indeed self-mode locking of the modes arises after some initial perturbation, e.g. with some tapping on the table.

The soliton laser made by Mollenauer and Stolen in 1984 was a coupled-cavity mode locked (CCM) laser. The main oscillator was an alkali halide cavity, synchronously pumped by an actively mode-locked krypton-ion laser. This main cavity was coupled through a 50% beam splitter to an external cavity that contained an optical fibre that had negative group velocity dispersion (GVD). The soliton laser achieved femtosecond pulse generation by using nonlinear optical feedback from the optical fibre in the external cavity. The non-linear phase shift of the fibre is an effect of self-phase modulation (SPM) and when the fibre pulse is recombined with the pulse in the master cavity leads to constructive interference near the peak of the pulse, while the wings of the pulse experience destructive interference. SPM is also connected to the

non-linear refractive index n_2 and is a phenomenon that leads to spectral broadening of optical pulses. Thus, APM can also be viewed as a fast saturable absorber. The CCM lasers are not very robust, the interference conditions must be continuously monitored and coupling into fibre is delicate.

Development into all-fibre laser systems using polarization APM has been reported both for soliton and non-solition lasers, [3], [4], respectively. Interest in all-fibre laser systems has increased because of the development in optical communication. It is an inexpensive compact source for generating ultrashort pulses and relative easy to set up.The solition laser, at high power levels the pulses exhibit dramatic changes in their shape and develop multipeak structure. The sensitive nature of soliton pulses limits it use for high-energy applications. However, stretched pulse from polarization APM fibre ring lasers have caught the attention, because of their ability to generate high-energy pulses comparable to color-center lasers. The stretched pulse laser is an all-fibre ring laser with two parts; one has positive dispersion and the other negative dispersion. The net dispersion of the cavity is slightly positive and is therefore able to work in the non-soliton regime. Theoretical models have been developed for pulse evolution in lasers that uses the effects of APM and KLM, [5].

The objective of this dissertation was to build a fibre ring laser as a part of my MSc. degree in Engineering Physics at the Royal Institute of Technology in Sweden. As the work started it grew to include a numerical model of the fibre ring laser and experimental measurements of the GVD. The built polarisation-rotation APM fibre ring laser will be used as a pump source for low threshold “chirped-crystal” optical parametric oscillation experiments to generate pulses with wavelengths in the 3 μm region. The parametric downconversion is possible with a highly positively chirped pump pulse (the fibre ring laser) incident on the crystal (which is aperiodically poled). It will also be used for two-photon microscopy of semiconductors.

The outline for the dissertation is as follows: first a numerical model of stretched pulse in the polarization APM fibre ring laser will be described in the first chapter. I will explain the mathematics and approximations that have been made in the model. Numerical simulation is only a tool to gain physical insight of the laser system and will be used as comparison between theory and experiment. The second chapter contains measurement and theory on GVD experiment. GVD is critical parameter for stretched pulse generation in the fibre ring laser and will be explained under this section; Third chapter will illustrate the experimental set-up of the fibre ring laser and tricks of the trade down to experimental result.

1 Numerical calculation

In telecommunications today, the silica glass fibre is the most used transmission medium for long- and short-distance communication. Propagation of optical fields within the fibres is governed by the Maxwell's equations, given by, [13]:

$$\begin{aligned} \nabla \times E &= -\frac{\partial E}{\partial t}, \\ \nabla \times B &= J_f + \frac{\partial D}{\partial t}, \\ \nabla \cdot D &= \rho_f, \\ \nabla \cdot B &= 0, \end{aligned} \qquad (1.1 - 1.4)$$

where E and H are electric field and magnetic field vectors, respectively. D and B are the related electric and magnetic flux densities. In a fibre the current density vector, J_f, is zero and also the charge density, ρ_f. D and B are related to E and H through the relations:

$$\begin{aligned} D &= \varepsilon_0 E + P, \\ B &= \mu_0 H + M, \end{aligned} \qquad (1.5, 1.6)$$

The flux densities are a consequence of the response of the dielectric, in the case the fibre. Thus, there is no magnetic polarisation, M=0. From equations (1.1) (by taking the curl), (1.5), (1.6) and the mathematical relation:

$$\nabla \times \nabla \times E = \nabla(\nabla \cdot E) - \nabla^2 E = -\nabla^2 E, \qquad (1.7)$$

we obtain the well known wave equation:

$$\left(\nabla^2 - \frac{1}{c^2} \frac{\partial^2}{\partial t^2} \right) E(x, y, z, t) = \mu_0 \frac{\partial^2}{\partial t^2} P(x, y, z, t), \qquad (1.8)$$

If the electric field is only manifested as a perturbation of the ground state of the material we can expand the macroscopic polarisation vector of a medium in a Taylor series so that the distinction between linear and non-linear regimes can be clearly shown, [7]:

$$\begin{aligned} P = \varepsilon_0 (& \chi^{(1)} \cdot E && \text{Linear optics: refractive index, absorption} \\ & + \chi^{(2)} \cdot EE && \text{Nonlinear optics: } 2^{\text{nd}}\text{-harmonic generation, parametric effects} \\ & + \chi^{(3)} \cdot EEE && 3^{\text{rd}}\text{-harmonic generation, non-linear index} \\ & + \ldots) \end{aligned} \qquad (1.9)$$

The second order susceptibility, $\chi^{(2)}$, is only nonzero if the dielectric lacks inversion symmetry in their atomic/molecular crystal structure. Since silica, $Si0_2$, has an amorphous structure $\chi^{(2)}$ vanishes. Thus, the lowest-order non-linear effect in a centrosymmetric medium is the third-order susceptibility, $\chi^{(3)}$, which is responsible for self-phase modulation, self-focusing, saturable gain and saturable absorption. Higher-order effects will not be considered here. The most important effect in optical fibres is the intensity dependent complex dielectricity constant, [6].

$$\varepsilon(\omega) = \left(\tilde{n} + i \frac{\tilde{\alpha}}{2k_0} \right)^2, \tag{1.10}$$

where

$$\begin{aligned} \tilde{n} &= n + n_2 |E|^2, \\ \tilde{\alpha} &= \alpha + \alpha_2 |E|^2, \end{aligned} \tag{1.11,1.12}$$

The second terms in equation (1.11) and (1.12) are a consequence of the third-order coefficient in the Taylor expansion of the polarisation vector, equation (1.9). Where $n_2 \propto \mathrm{Re}[\chi^{(3)}]$ is the non-linear refractive index and $\alpha_2 \propto \mathrm{Im}[\chi^{(3)}]$ is the two-photon absorption coefficient. Since α_2 is relatively small for silica fibre compared to α (absorption), it is taken to be zero. Further, n (refractive index) and α are the real and imaginary part of the first-order susceptibility, $\chi^{(1)}$, which corresponds to the linear optics stated in equation (1.9). If only one pulse is incident on the sample the corresponding polarisation, assuming an instantaneous response, can be written, [8]:

$$P^{(3)}(t) = \varepsilon_0 \chi^{(3)} \left(\frac{3}{8} |E|^2 E(t) \exp(i\omega_l t) + \frac{1}{8} E^3 \exp(3i\omega_l t) \right) + c.c., \tag{1.13}$$

where ω_l is the centre frequency. The second term with $3\omega_l$ in the exponential describes third harmonic generation, but in many optical materials this process is not effective and will not be considered. From equation (1.11) it can be shown that:

$$n_2 = \frac{3\chi^{(3)}}{8n}, \tag{1.14}$$

The real part of equation (1.10) is then the linear and the non-linear refractive index, while the imaginary part is only the linear absorption. The intensity dependence of $\tilde{n}$ implies refractive index varying in time and space. When an applied electric field is strong enough the electronic cloud of an atom or a molecule is strongly distorted. This happens when the mean electrostatic energy of the field $1/2\varepsilon_0\chi^{(3)}\langle E \cdot E \rangle E \cdot V$ (V being the interaction volume) becomes comparable to the energy of the electronic states. This leads to different effects, such as self-phase modulation (SPM), a phenomenal that leads to spectral broadening of optical pulses. SPM is the temporal analogue of the spatial self-focusing effect (Kerr lens), explained in the *Introduction*.
The effect of non-linear propagation of a light pulse is a complex problem that needs numerical solutions. To get a feeling for SPM and the Kerr effect, a short simplified explanation will be given here.

Kerr lens Effect

We start with the spatial dependence of the light intensity and by assuming a Gaussian laser beam in a $\chi^{(3)}$ material. The Gaussian function describes the intensity distribution with its shape parameter w. In this case equation (11) becomes:

$$\tilde{n}(r) = n + n_2 I(r), \quad I(r) = I_0 \exp\left(-(\frac{r}{w})^2\right), \tag{1.15}$$

When this beam propagates through a $\chi^{(3)}$ material, the index change follows the intensity along the Gaussian function *I(r)*. The beam will feel a higher refractive index at r=0 than in its wings and while propagating the optical path lengths will differ from the centre of the beam and its wings. Assuming that $n_2>0$ it will act as a positive lens and focus a collimated beam. When a pulse propagates through a thick material this process is intensified along the path because focusing of the beam increases the dynamic refractive index and therefore increases the focal power of the Kerr lens. This increase of the focusing lens stops when the diameter of the beam is small enough and the linear diffraction is large enough to balance the Kerr effect. This is the effect for self-mode locking or Kerr lens mode locking (KLM).

Self-phase modulation

Consider a plane wave propagating in a non-linear material:

$$\begin{aligned} &E(t,z) = E_0 \exp\big(i(\omega_0 t - k(t)z)\big), \\ &\phi(t) = \omega_0 t - k(t)z, \end{aligned} \qquad k(t) = \frac{\omega_0}{c}\tilde{n}(t), \tag{1.16}$$

The dynamic refractive index is now assumed to be time-dependent, where the light pulse envelope is assumed to be a Gaussian function of time.

$$\tilde{n}(t) = n + n_2 I(t), \quad I(r) = I_0 \exp\left(-(\frac{t}{\tau})^2\right), \tag{1.17}$$

SPM-induced spectral broadening is a consequence of the time dependence of the phase in equation (1.16). When the pulse passes, the phase will temporally vary which implies that the optical frequency changes across the pulse from its central value ω_0. The time derivative of the phase gives the instantaneous frequency and can be written as:

$$\begin{aligned} &\omega(t) = \frac{\partial}{\partial t}\phi(t) = \omega_0 - \frac{\omega n_2}{c}\frac{\partial I(t)}{\partial t}z, \\ &\Delta\omega(t) = \omega(t) - \omega_0 = -\frac{\omega n_2}{c}\frac{\partial I(t)}{\partial t}z, \end{aligned} \tag{1.18,1.19}$$

where equation (1.19) gives the frequency variation over the pulse. It can be understood from equation (1.19) that the self-phase modulation creates, with $n_2>0$, new low frequencies in the leading edge of the pulse envelope and new high

frequencies are created in the trailing edge. The time dependence of $\Delta\omega(t)$ can be viewed as a frequency chirp. The chirp is induced by SPM and increases in magnitude with the propagated distance and has a form that is dependent on the pulse shape.

Non-linear Schrödinger equation

SPM and the Kerr effect are the basis of the polarisation additive pulse mode locking (P-APM) technique and are implemented in the wave equation (1.8). It is more convenient to work in the Fourier domain, i.e. by Fourier transforming equation (1.8) and treat the intensity dependent dynamic refraction index term (i.e. equation (1.11)) as a constant during the transform. This is feasible under the slowly varying envelope approximation (SVEA) for E(r,t), by separating the rapidly varying part of the electric field in equation (8), i.e. $E(r,t)=1/2[U(r,t)\exp(-i\omega_o t)+c.c.]$, (1.20). Where U(r,t) is a slowly varying function of time relative to the optical period. Fourier transforming equation (1.20) and using the method of variable separation.

$$\widetilde{E}(r,\omega-\omega_0)=\widetilde{F}(x,y)\widetilde{A}(z,\omega-\omega_0)\exp(i\beta_0 z), \tag{1.21}$$

where $\tilde{A}$ is the slowly varying function of z, β_0 is the wavenumber and $\tilde{F}(x,y)$ is the modal distribution function. With equation (1.21) in the Fourier transformed wave equation it gives two coupled solutions to the wave equation. With SVEA it reduces the wave equation to first-order derivatives with respect to the spatial propagation direction z. Further simplification are made by using first-order perturbation theory to the modal distribution function F(x,y) from where the eigenvalue is determined. The non-linear refractive index and the absorption term do not then affect the modal distribution function F(x,y). Inverse Fourier transforming $\tilde{A}$ back in to the time-domain, the non-linear Schrödinger equation can be written as follows (see reference [6] for details):

$$\frac{\partial A}{\partial z}+\beta_1\frac{\partial A}{\partial t}+\frac{i}{2}\beta_2\frac{\partial^2 A}{\partial t^2}+\frac{\alpha}{2}A=i\gamma|A|^2A, \tag{1.22}$$

where β_1 and β_2 are the group velocity and the GVD, respectively. The non-linear coefficient γ is defined as:

$$\gamma=\frac{n_2\omega_0}{cA_{eff}}, \tag{1.23}$$

where A_{eff} is the effective core area and is usually approximated to be $A_{eff}=\pi w^2$, where w is the width parameter that dependent on the fibre parameters, [6]. As a consequence, the coupled wave equation F(x,y) is not needed in the calculations and the physical insight of pulse propagation in the fibre ring laser will not be lost. Equation (1.22) then describes the propagation of an optical pulse in single-mode fibre and is referred to as non-linear Schrödinger equation. *A* is the pulse amplitude and is assumed to be normalised so that $|A|^2$ is the optical power. γ has the units of $w^{-1}m^{-1}$. By making the transformation:

$$T = t - \frac{z}{v_g} = t - \beta_1 z, \tag{1.24}$$

and using equation (1.22), we obtain:

$$\frac{\partial A}{\partial z} + \frac{i}{2}\beta_2 \frac{\partial^2 A}{\partial t^2} + \frac{\alpha}{2} A = i\gamma |A|^2 A, \tag{1.25}$$

and is called the retarded frame. The frame of reference is then moving with the pulse at its group velocity v_g. It makes it easier to implement in a program for numerical solutions. Equation (1.25) is the standpoint from which the numerical model is based upon.
The fibre ring laser has three different fibres: SMF28, 980/1550 WDM coupler and highly doped Erbium fibre. All these fibres have different GVD parameters, absorption coefficients, non-linear coefficients and, for the Erbium fibre also, a gain coefficient.

Gain coefficient in the Erbium doped fibre

The discovery of erbium is generally credited to Carl G. Mosander, he found it in Ytterby, Sweden, in mid 19-century. But it was not until 1934 it was isolated in a fairly pure form. In the late 1980s the development of rare earth dopands, such as Er and Nd, in fibre lasers really took off. This was due to the rapid evolution in telecommunication systems. Mode-locked Er-doped fibre lasers were of special interest, because it could produce pulses in the 1.55 μm region.

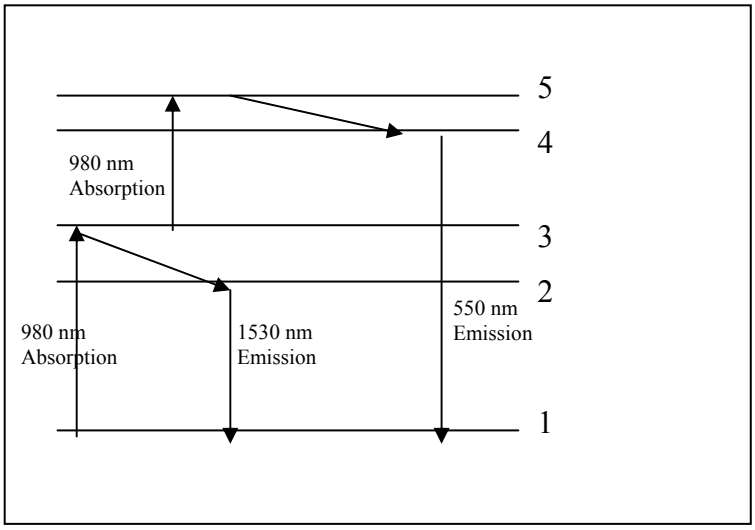

Figure 1.1.

Erbium is a three-level atomic system and acts as the gain medium in the P-APM fibre ring laser. Trying to explain the mechanism behind the amplifying medium one must make a few assumptions without losing the physical relevance.

Theoretical models for calculating susceptibility for Erbium doped fibres have been done with a semiclassical approach described in [9]. We proceed by applying some of the results from [9] and starting from a classical viewpoint, so that the physics behind the gain medium doesn't get lost. First, by looking at the simplified energy level diagram over Erbium, Figure 1.1, and writing the rate equation for the energy levels shown:

$$\begin{aligned} \frac{dN_3}{dt} &= P_{pump} N_1 - P_{32} N_3 - P_{31} N_3 - P_{35} N_3, \\ \frac{dN_2}{dt} &= P_{32} N_3 - P_{21} N_2, \end{aligned} \tag{1.26}$$

Where P_{pump} is the transition probability per unit time, which accounts for both the absorption cross-section of the material and the intensity of the incoming light. The P_{35} term is the excited state absorption and will not effect the overall amplifier performance and will be set to zero. From state 3, electrons can decay either to state 2 with probability P_{32} or to the ground state with probability P_{31}. We assume that the transition probability $P_{32} >> P_{31}$ and that state 2 has a large lifetime compared to state 3 ($P_{21} << P_{32}$). In Erbium state 2 has a lifetime about 10 ms. A steady state dynamical behaviour is a solution to equation (1.26) and corresponds to a constant state population with time, so the derivatives vanishes and gives:

$$\frac{N_2}{N_1} \approx \frac{P_{pump}}{P_{21}} \left(1 - \frac{P_{31}}{P_{32}} \right), \tag{1.27}$$

When $N_2 > N_1$ occurs the population is inverted, which enables laser operation. This is reached when (i) the pumping rate is large enough, (ii) the electronic decay from the state 3 to state 2 is faster then to any other decay, (iii) the metastabel state, i.e. state 2, is substantially over occupied. Once a population inversion is established, the Erbium-doped fibre can amplify light. However, there are some limits to how much the light can be amplified. Consider a low-intensity electromagnetic wave propagating along z with a gain proportional to the population inversion $\Delta N = N_1 - N_2$ and to the wave intensity.

$$\frac{dA(z)}{dz} = -A(z) \cdot \Delta N \cdot \sigma_{21}(\omega), \tag{1.28}$$

where $\sigma_{21}(\omega)$ is the emission cross-section of the transition between state 2 and 1.

From previously stated assumptions one can re-write equation (1.27) with $\Delta N=N_1-N_2$ and by replacing the probabilities by energies (because they are only involved in ratios) gives:

$$\Delta N \approx -N_2 \frac{1}{1+\frac{E(z)}{E_{sat}}}, \tag{1.29}$$

Introducing equation (1.29) into (1.28) with $g(\omega)=N_2\sigma_{21}(\omega)$ we obtain:

$$\frac{dA(z)}{dt} = \frac{A(z)\cdot g(\omega)}{1+\frac{E(z)}{E_{sat}}}, \tag{1.30}$$

where E_{sat} is the energy saturation term and is calculated from the time integral of $|A|^2$. A typical value of E_{sat} is about 3 μJ, [6].

The gain profile, $g(\omega)$, is in many textbooks, for example [6], is approximated with a Lorentzian profile, which is not observed in Erbium doped fibre, [9]. We will us the measured gain profile for the Erbium doped fibre, given by Fiber Core Ltd. In figure 1.2 the gain and absorption profile is shown. Other interesting effects take place in the Erbium doped fibre. When including the effects of dopants to the induced polarisation vector in the right hand side of equation (1.8) they will contribute to the complex dielectricity term (1.10). Because of the finite gain bandwidth, all spectral components do not experience the same gain, which is referred to as gain dispersion. And also, if the carrier frequency of the incident field does not coincide with the gain peak located at 1530 nm, see Figure 1.2, it will undergo a refractive index change. The non-linear Schrödinger equation is valid for pulse-widths longer than the dipole relaxation time, $T_2 \approx 0.1$ ps, of the doped fibre. Since the stretched pulses that are generated in the fibre ring laser have durations about $T \approx 1$ - 5 ps, one can relax the Maxwell-Bloch equations [6]. The additional term in for the gain dispersion and refractive index change in equation (1.10) is given by [10] in the Fourier domain. The interesting part is the second-order coefficient in the Taylor expansion of the susceptibility of a two level system given by

$$\tilde{\chi}^{(2)}_{dopants} = \frac{g}{2n_0}\frac{\delta(\delta^2-3)+i(1-3\delta^2)}{(1+\delta^2)^3}(\omega-\omega_0)^2 T_2^2, \tag{1.31}$$

where $\delta=(\omega_0-\omega_a)T_2$ is the detuning parameter and ω_0 is the carrier frequency, with the related linear refractive index n_0. ω_a is the frequency corresponding to the gain peak, (see Figure 1.2) and g is the frequency dependent gain constant.

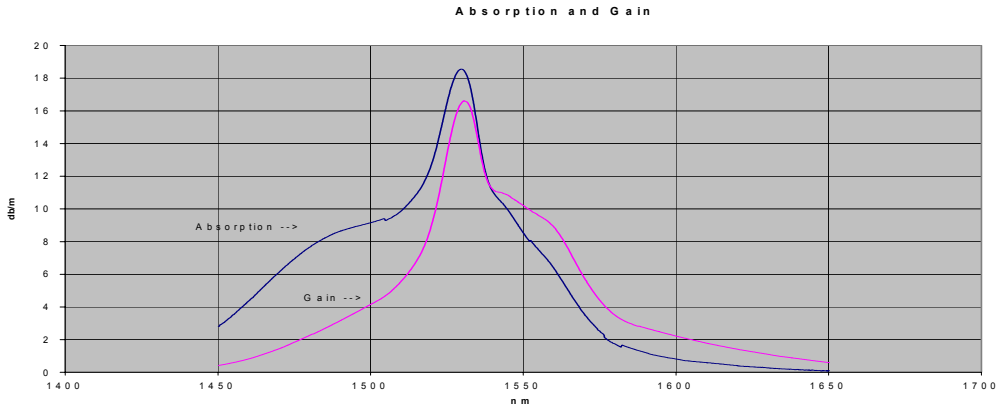

Figure 1.2. (Courtesy of Fibre Core Ltd.)

The real part of equation (1.31) is the refractive index change and the imaginary part is the gain dispersion. These results, though, do not coincide with experimental calculations made by [9], which assume a three level system. This implies that the approximation to a two level system in [10] doesn't give the desired accuracy. The gain dispersion is accounted for in the gain spectrum seen in Figure 1.2 and so the imaginary part of equation (1.31) could be dropped. The refractive index change over the spectrum can be calculated from the Kramers-Kronig relations with the Erbium doped fibre spectral gain, [9]. But instead of calculating one could make a qualified guess and try to fit a curve to the results given by [9]. $\Delta n(\omega)$ is dependent on the gain profile and the pump power and has a characteristic profile that can be viewed in Figure 1.3.

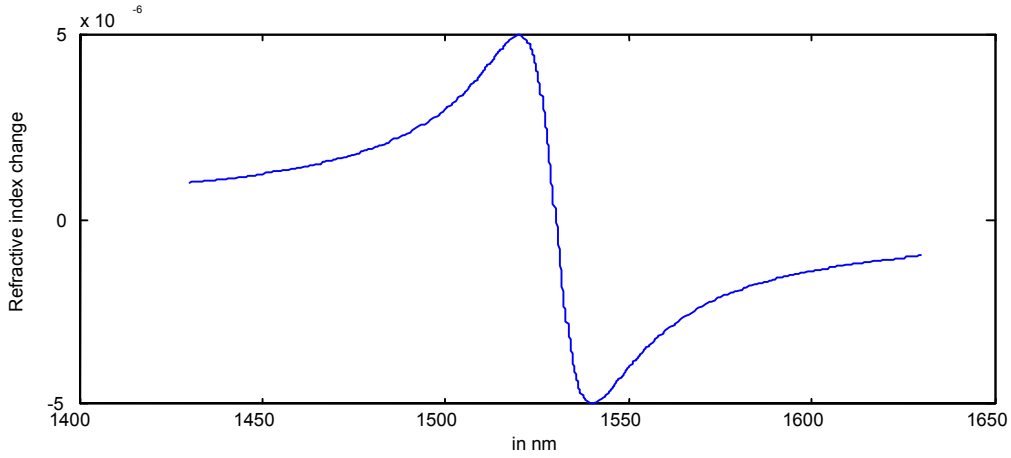

Figure 1.3.

The profile can be written as a mathematical function given by:

$$\Delta n(\omega) = G'(\omega) \cdot \frac{\varpi}{(1+\varpi^2)}, \qquad (1.32)$$

where $\varpi=(\omega_0-\omega)T_2$ is the normalised frequency to the dipole relaxation time, ω_0 is the gain peak frequency and G'(ω) is the normalised gain spectrum, in Figure 1.3 set to

unity. The fibre ring laser is back-pumped, which means that the gain increase while propagating through the Erbium doped fibre. To simulate this, [11] applied an exponential function to the gain spectrum:

$$G(z,\omega) = G'(\omega)\cdot \exp\left(\frac{z}{z_a}\right), \tag{1.33}$$

where z_a is a constant chosen so that the ratio between the length of the Erbium fibre and z_a is 4/3, [11]. Putting the results from equation (1.33) into (1.32) and replacing the real part of equation (1.31), we arrive at the following result:

$$\tilde{\chi}^{(2)}_{dopants} = \frac{G(\omega)}{2n_0}\cdot\frac{T_2^2\varpi}{(1+\varpi^2)}(\omega-\omega_0)^2, \tag{1.34}$$

where the Taylor expansion has been made around ω_0. The coefficients in front of $(\omega - \omega_0)^2$ have the units of ps^2/m, same as the GVD parameter.

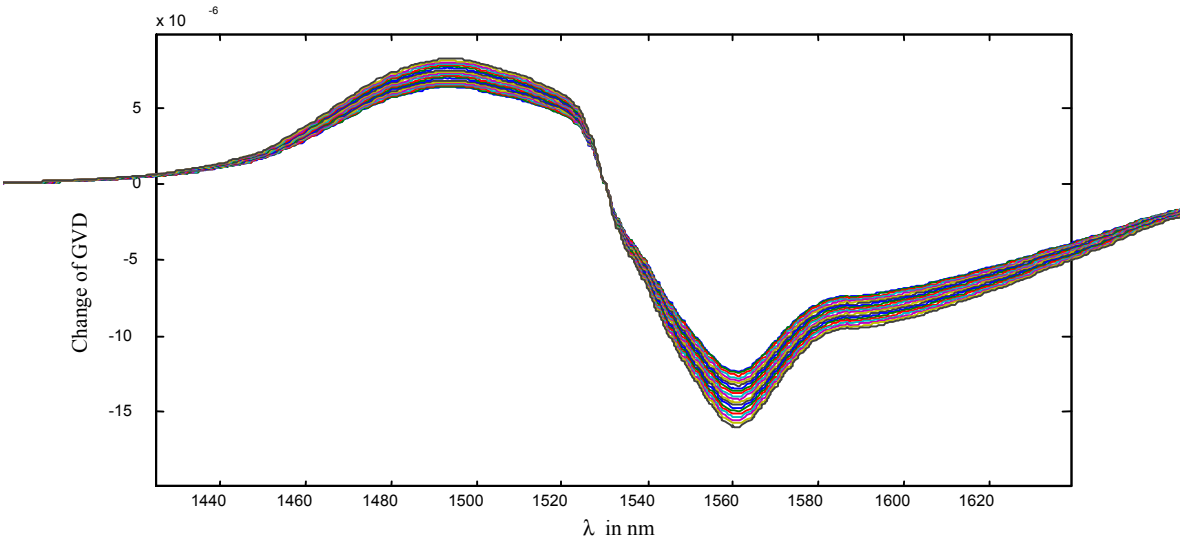

Figure 1.4.

In Figure 1.4 equation (1.34) is shown over the spectral range and it coincides well with calculation in [9]. It is a qualitative graph where the index change is view over the spectrum and the impact of the backward pumped fibre. The pulse will encounter higher gain the further it propagates through the Erbium doped fibre, thus it affects the $\Delta n(\omega)$ around the carrier frequency so that the amplitude becomes larger. This happens, as seen in Figure 1.4, mostly in the leading and trailing edge of the spectrum. However, the change over the spectrum is not very large compared to the GVD of Erbium. Reference [9] implies that it is negligible for one pass through the doped fibre. In our case, the fibre ring laser simulations will conduct about 300 - 700 roundtrips and the refractive index change will have an impact on the solution.

Finally, the non-linear Schrödinger equation for the Erbium doped fibre can be written as, were equation (1.34) is written in the time domain:

$$\frac{\partial A}{\partial z}+\frac{i}{2}(\beta_2+\chi^{(2)}_{dopants})\frac{\partial^2 A}{\partial t^2}+\frac{\alpha}{2}A=i\gamma|A|^2A+\frac{G}{1+\frac{E(z)}{E_{sat}}}A, \qquad (1.35)$$

Equation (1.35) describes pulse propagation in doped optical fibre. When A is in the CW regime the non-linearity becomes very small and (1.35) is relaxed to the regular wave equation with a gain term. So there is no need for two equations, i.e., one for pulse operation and one for CW operation. From here it is necessary to find a way to simulate the mode-locking mechanism of the P-APM.

Passive Mode locking in the fibre ring laser

The unidirectional laser has two polarisation controllers that provide the basis for mode locking. The first polarisation controller changes the polarisation to circular. The different polarisation states then propagate non-linearly through the fibre, due to the Kerr effect. The second polarisation controller sets the polarisation so that the most intense part of the light is transmitted into the cavity for another round trip. Which is the fast saturable absorber. This is the mechanism that needs to be simulated. Under the third section the mode locking mechanism will be thoroughly explained for the fibre ring laser. In [12] the following mathematical description of a fast saturable absorber was made:

$$S(|A|^2)=a+b\tanh\left(F_{speed}(|A|^2-P_{Thres})\right), \qquad (1.36)$$

where a and b are constants to be set in a proper way and usually a>b. F_{speed} is the speed of the saturable absorber and P_{thres} is the power threshold for the laser. To give and example we chose a=0.8, b=0.1, P_{Thres}=5 and F_{speed}=1,5,10. Higher F_{speed} gives faster saturable absorber response. a and b is then adjusted so that desired output coupling is achieved and the threshold is chosen so that it gives mode locking at desired input pump power. Given in Figure 1.4.

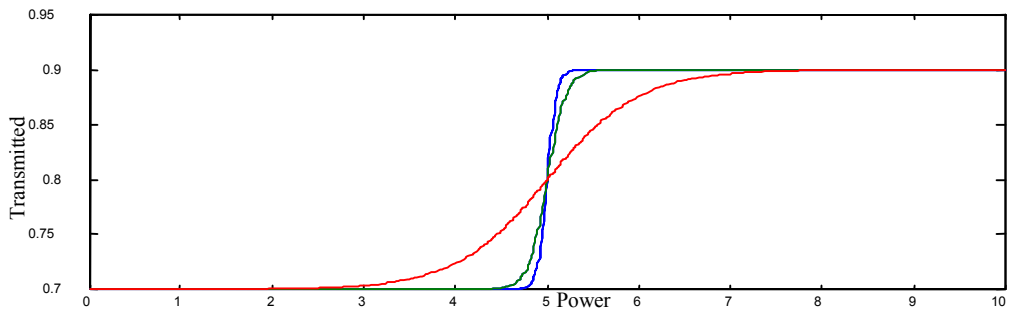

Figure 1.5.

The square of equation (1.36) is then multiplied with the amplitude A to pass the most intense part of the light for another roundtrip in the laser. The residue of (1.36) is the output and is coupled out of the cavity.

Now when all the theory and approximation is done, we need a numerical method to solve this. In equation (1.25) and (1.35) there are some of the components that are given in the Fourier domain (gain and refractive index change) and some in the time domain (non-linear refractive index), and to take into account all this, a powerful method must be used. One suitable method is the split-step Fourier method, [6].

Split-step Fourier method

What is basically done is separation of the non-linear part from the linear part in equation (25) and (35) so that we get two equations:

$$\frac{\partial A}{\partial z} = -\frac{i}{2}(\beta_2 + \chi^{(2)}_{dopants})\frac{\partial^2 A}{\partial t^2} - \frac{\alpha}{2}A,$$
$$\frac{\partial A}{\partial z} = i\gamma|A|^2 A + \frac{G}{1+\frac{E(z)}{E_{sat}}}A, \qquad (1.37,1.38)$$

where (1.37) is the linear part of (1.35) and (1.38) is the non-linear part, respectively. For the SMF28 and 980/1550 WDM coupler, the gain, G, and $\chi_{dopants}$ is zero. GVD and non-linearity usually work together along the fibre length. In the split-step Fourier method the dispersive and non-linearity effects work independently over a small step size h and give an approximate solution. Propagation from z to z+h is done in two steps: (i) the non-linearity acts alone and right side of (1.37) is set to be zero. Equation (1.38) is then solved with a Runge-Kutta method with the boundary condition. (ii) the right side of (1.38) is set to zero and (1.37) can be Fourier transformed by replacing the differential operator ∂/∂t by iω and solving the expression analytically, resulting in:

$$\tilde{A}(z+h,\omega) = \tilde{A}(z,\omega)\exp\left((\frac{i}{2}(\beta_2 + \chi^{(2)}_{dopants})\omega^2 - \alpha)h\right), \qquad (1.39)$$

where A˜(z,0) is calculated in step (i). Where the step size h is added.

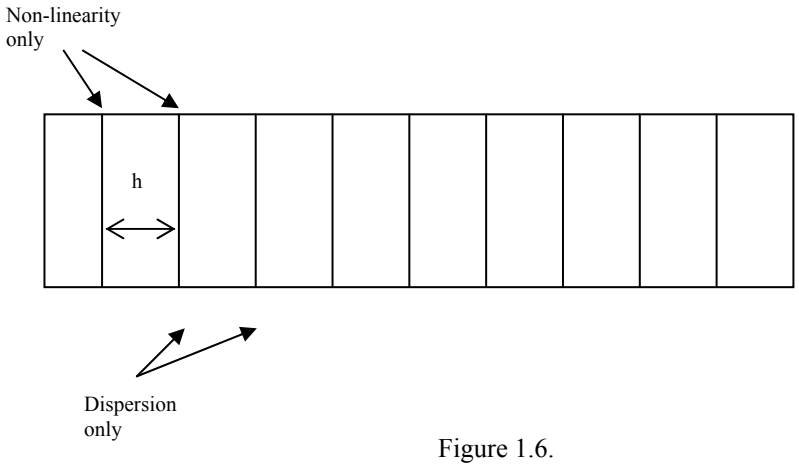

Figure 1.6.

To put the split-step Fourier method into practice is quit straightforward. As shown in Figure 1.6, the fibre length is divided into a large number of segments that are equally spaced. Following the steps (i) and (ii) the optical pulse is propagating from segment to segment. Using the fast Fourier transform (FFT) algorithm in the software package MatLab, makes the numerical calculation of (1.39) relatively fast. The split-step Fourier method is accurate to second order in the step size h, [6], which is good enough for these calculations. When solving the non-linear part of the doped fibre two additional steps are required in the Runge-Kutta method, because of the fact that the gain parameter is given in the Fourier domain. These lead to a split of (1.38) in to additional two parts, where the gain parameter is solved first without the non-linear coefficient γ in the Fourier domain and then follows the step (ii). After this, the non-linear coefficient is included and $G(\omega)$ is set to zero and solved again according to step (i). These approximations will affect the accuracy, but not appreciably.

Numerical calculations

To estimate the accuracy and validity of the numerical model and of its different components, such as SPM, GVD and gain, it was necessary to apply the model to known results. The results given by [6] on SPM and GVD is well accounted for in the model and also the results on pulse propagation in gain material coincide with results given by [11]. As mentioned before, the laser contains of two sections, one with negative GVD (SMF28 and 980/1530 WDM coupler) and one section with positive GVD, which is the gain section. The fast saturable absorber, given above, will also act as a rejection port for the laser, from where the output pulse will be calculated. A critical parameter is the dipole relaxation time, T_2, which indicate when the Maxwell-Bloch equation can be relaxed. The stretched pulses have a pulse length of about 1 - 5 ps and hence the Maxwell-Bloch equations can be relaxed. T_2 is the time it takes for the molecules in the silica fibre to align to the incoming polarisation state of the pulse. Under perfect conditions it is plausible to assume that only one polarisation state is present in the laser and there will be no need to include cross-phase modulation (XPM). In Figure 1.7 a sketch of the simulated ring laser is shown.

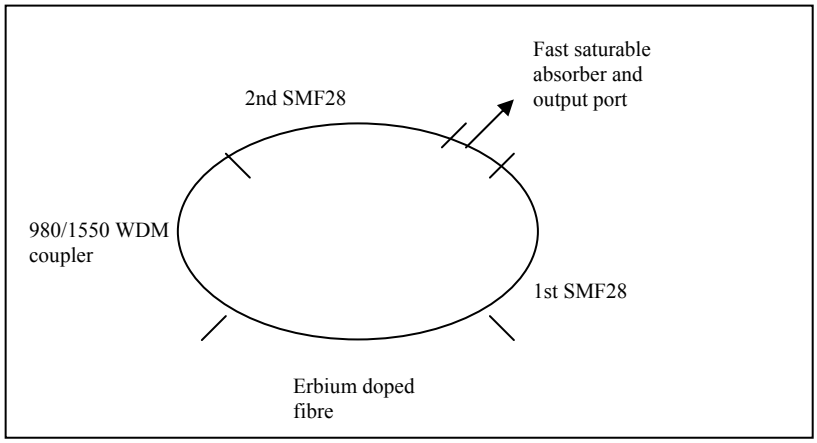

Figure 1.7.

The Erbium is assumed to be in steady state and have a well over populated metastable state and the pulse will propagated in the clockwise direction. A flow chart for the program when implemented in the software package MatLab can be viewed in Figure 1.8.

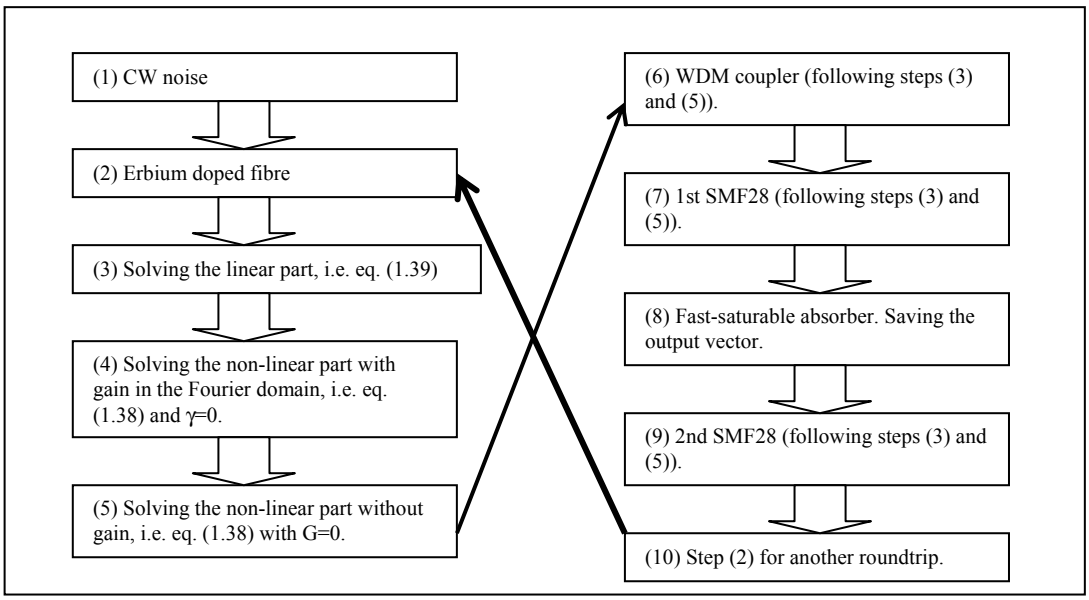

Figure 1.8.

The input to the laser is CW noise that will propagate through the laser and generated a pulse when it reaches the threshold for the saturable absorber. The noise is randomly generated in MatLab and is set to an average power about 100 μW. All the parameters used in the program were either calculated experimentally or given from literature and articles, except the saturable absorber parameters. The important GVD parameter for the different fibres used in the simulation where measured with a technique called dispersive Fourier transforms spectroscopy (DFTS) and will be considered in the next section. The gain coefficient and spectrum were interpolated from the Figure 1.2 and implemented into the program. The different non-linear coefficients, γ, were given by [6] and [11], and the measured threshold for mode locking was ~18 mW. Even though all these constants were given, a vast number of simulations were done before a satisfactory result was given. Usually about 200-400 roundtrips were conducted in order to get a mode locked pulse.

Calculated results

Running this program was very time consuming (300 roundtrips could take up to 2.5 hours), and therefore I was forced to seek the knowledge of the fibre ring laser's characteristics and not for the coincidence with former experimental results on similar lasers. The two parameters that are interesting here and can be easily adjusted in a laboratory are the net dispersion of the cavity and the launched pump power. These are the features that will be illustrated here.

Gain

When varying the gain coefficient in the program, i.e., simulating the launched power in to the erbium-doped fibre, it was clearly seen that with higher gain the program reached mode locking faster than with lesser gain. Further, also an increase in the pulse energy was obtained. However, the pulse could not stay stable due to too high pulse energy and as a consequence, it developed multi-pulses, seen in Figure 1.9. The top plot has the highest gain, and then in decreasing order.

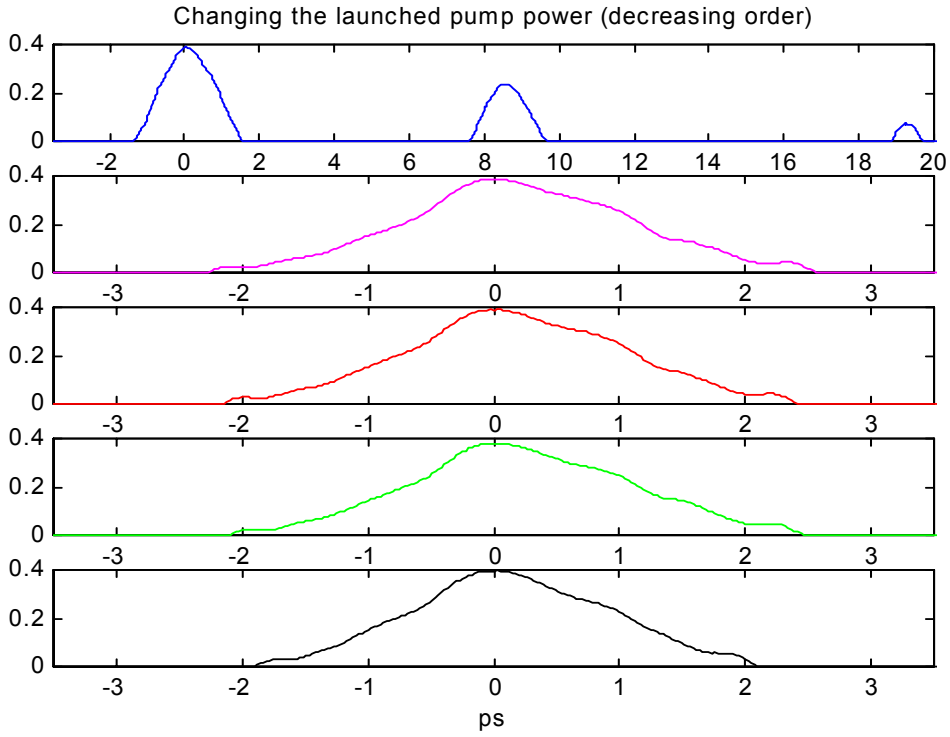

Figure 1.9

As can been seen, in Figure 1.9, the FWHM of the pulse decreases with higher gain. This is the consequence of the higher non-linearity's present, which increases the spectrum and shortens the pulse. Even so, there is an increase in the pulse energy and as an affect the leading and trailing edge of the pulse becomes broader. This is can be explained by the refractive index change, see equation (1.34), that is proportional to the gain coefficient. The amplitude of equation (1.34) increases, and will contribute to also increase the GVD for these spectral components and as a consequent the pulse leading and trailing edge becomes larger. Further, this leads also to new frequencies generated by SPM. Figure 1.10 illustrates the spectrum of Figure 1.9, it is not as obvious but the spectrum is wider in the second top plot.

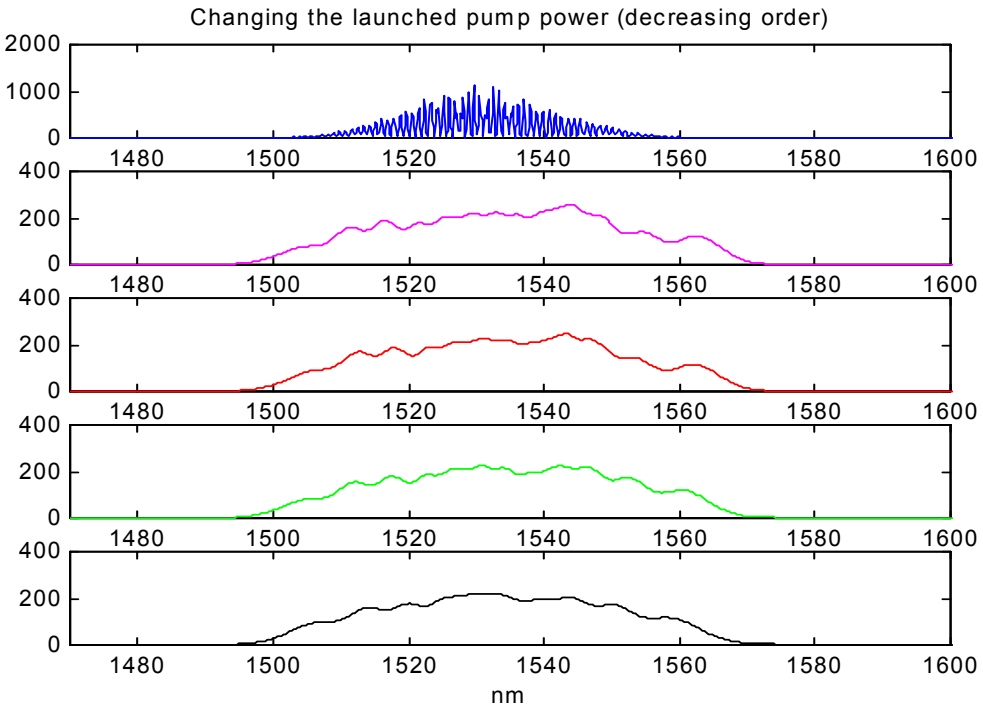

Figure 1.10.

The top plot in Figure 1.9 is not a splitting of a pulse, instead it can be understood as three different modes has gained sufficiently high energy to penetrate the fast saturable absorber. In experiments usually a pulse splits up in two or more, so what we see here is a consequence of the program and not what will happen in reality. With a higher gain constant the program mode locked fast, but on the other hand it becomes unstable.

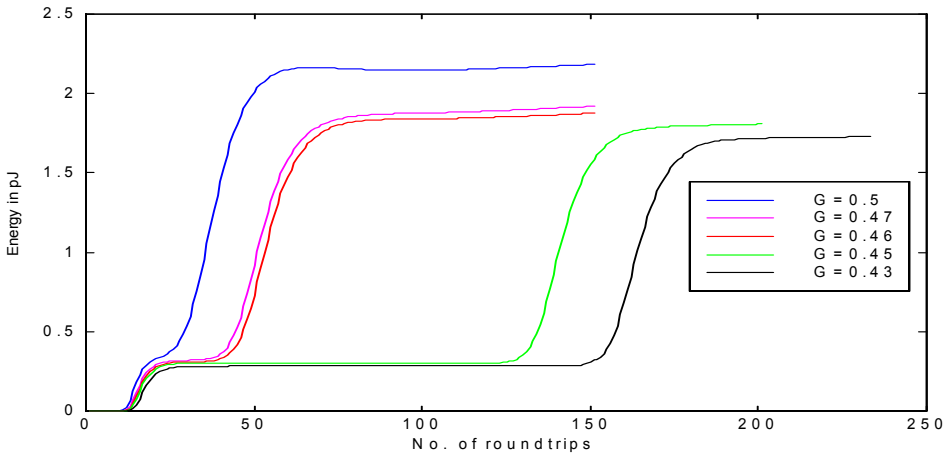

Figure 1.11

Figure 1.11 shows that relation between numbers of roundtrips conducted and pulse energy. The program starts from noise and amplifies so that a CW is reached (seen as a horizontal line), then when a CW spikes has accumulated sufficient energy it can penetrate the fast saturable absorber and becomes mode locked (seen as a rapid increase in energy).

The pulse saturates and becomes stable. For G=0.5 it goes from noise up to mode locking almost immediately and as a consequence multi-pulses develops.

Dispersion

This is the most important parameter and is the one that ultimately determine the pulse and spectrum. When calculating various net dispersions the gain was kept at G=0.45. With a net dispersion close to zero a very broad spectrum and low pulse energy is obtained. Increasing the net dispersion leads to faster mode locking and higher pulse energies. This can be seen in Figure 1.12.

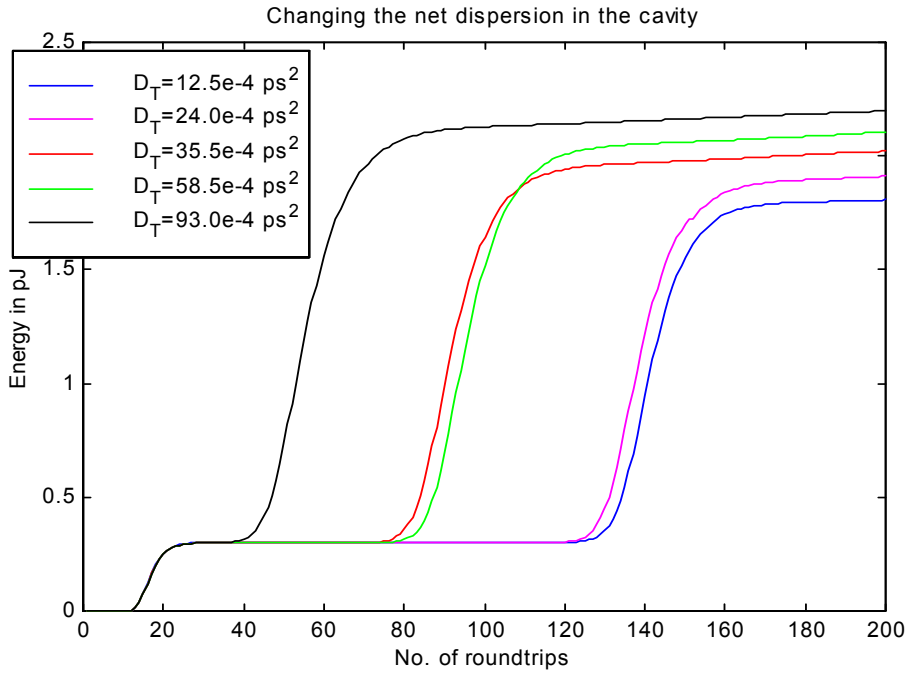

Figure 1.12

With higher positive net dispersion the program needs lesser roundtrips to obtain mode locking, which implies that energy transfer from the gain medium to the propagating beam is more efficient and therefore reaches mode locking faster. When the net dispersion increase the pulse width becomes broader, hence more energy can be store in the pulse. Other effect is that the non-linear effects become smaller due to lower peak intensities and as a consequence the spectrum becomes smaller and the SPM does not generate new frequencies in the leading and trailing edge of the spectrum.
In Figure 1.13 shows the pulses at the different net dispersions. A small decrease in the length of the single mode fibre results in a broadening of the pulse. In these simulations optimisation of the pulse energy can be calculated in order to extract the highest efficiency of the laser. At the top plot of Figure 1.13 the intra-cavity pulse width approaches the dipole relaxation time, T_2, which implies that the Maxwell-Bloch equations should be included, and this is maybe why the pulse profile is asymmetric in it appearance or that the step size in time and space is too large. Since running this program takes up to 3 hours there is no time to look into this matter at this point.

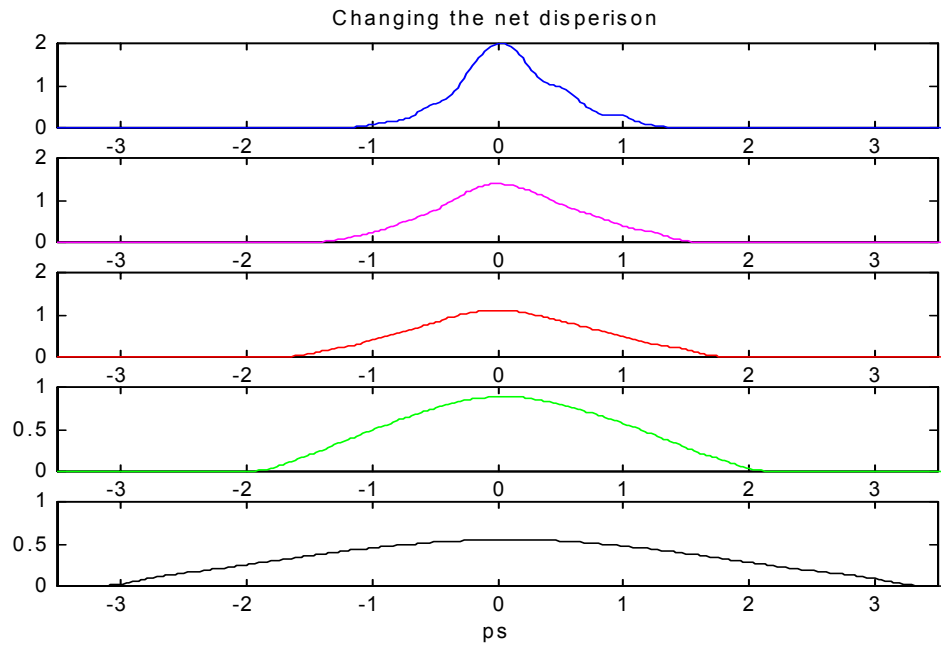

Figure 1.13

Figure 1.14 shows the corresponding spectrum. In the top view is the SPM clearly shown as a broadening of the spectrum.

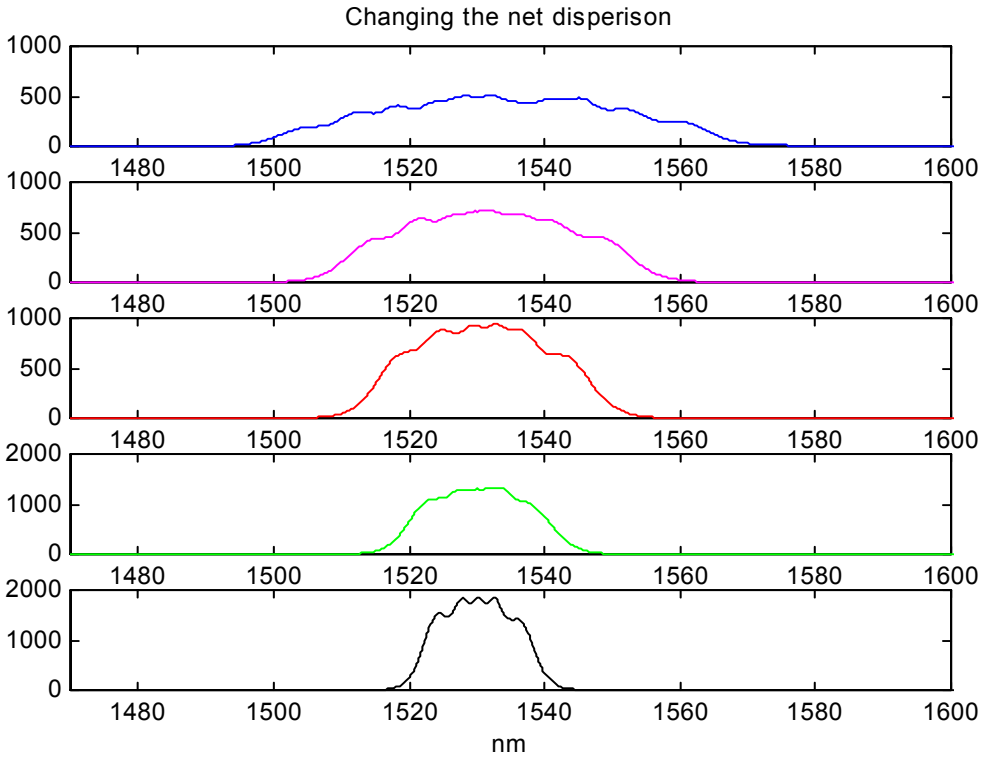

Figure 1.14

With decreasing length of the negative single mode fibre, the spectrum becomes smaller and the non-linear effects become almost absent. However, it is possible to

increase the non-linear coefficient γ, so a broader spectrum can be obtained. But here I am more interested in the relative change and not to be exact in my calculations. This shows that with higher positive net dispersion more energy can be obtain per pulse and the physical insight is noted.

Other interesting features is that it is possible to look at the pulse inside the cavity and thus, provide a opportunity to design the cavity in such way that maximum pulse energy and lower non-linearity's can be obtained for same pump power and net dispersion. In Figure 1.15 shows the mode locked pulse for G=0.45 and D_T=12.5e-4 during 1 roundtrip in the cavity.

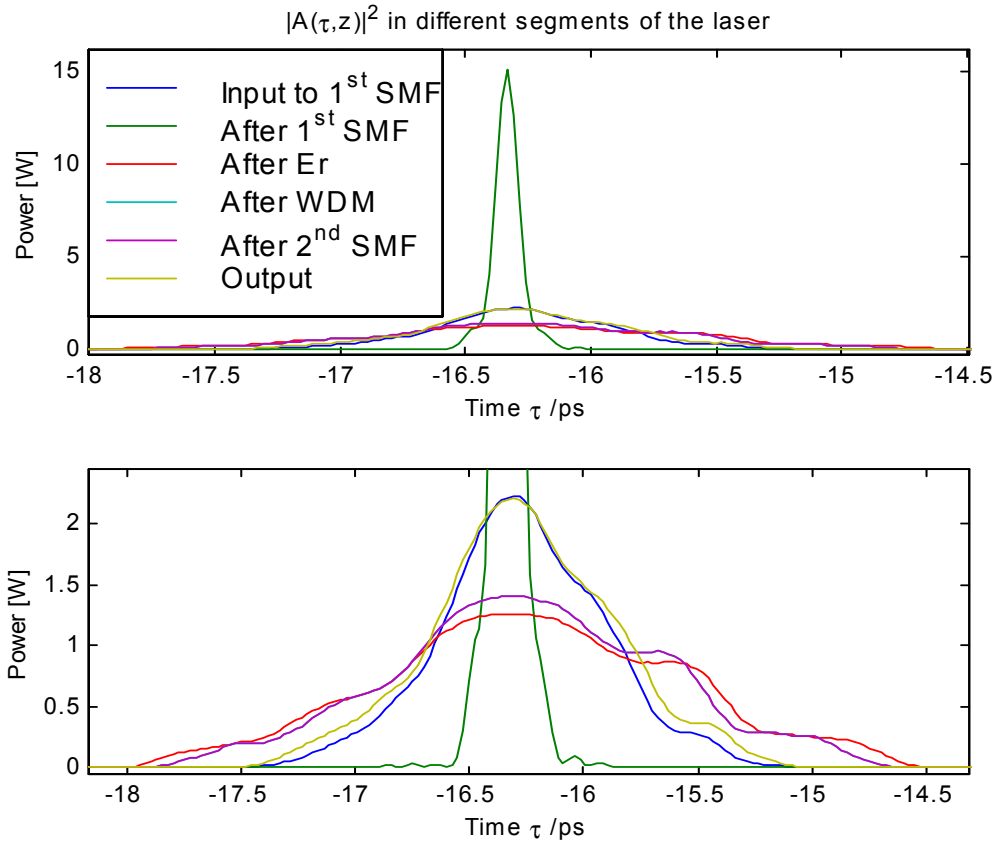

Figure 1.15.

After the first SMF the pulse has become narrower and higher peak power is obtained, the pulse width is very close to the dipole relaxation time, T_2, and this indicates that the Maxwell-Bloch equations should be calculated. The non-linearity's is then very high when it propagates in to the erbium-doped fibre (which has higher γ than SMF) and new frequencies will be generated. This is when usually pulses split up, because the dispersion cannot compensate the SPM. Further, when the narrow pulse propagates through the erbium-fibre it broadens because of the positive GVD and can therefore absorb more energy. The pulse broadens in an order of magnitude as can be seen in Figure 1.15 and when the pulse reaches the rejection port after a full roundtrip it has become narrower again because of the WDM coupler and the second SMF that has a negative GVD.

By “cutting” off some of the first SMF and place it in the second SMF, without changing the net dispersion of the cavity, it is feasible to lower the peak intensity’s within the cavity and as a consequence lowering the non-linearity.
In Figure 1.16, 50 cm of the first SMF has been “cut” off and “spliced” onto the second SMF and as a result the peak intensity has decreased.

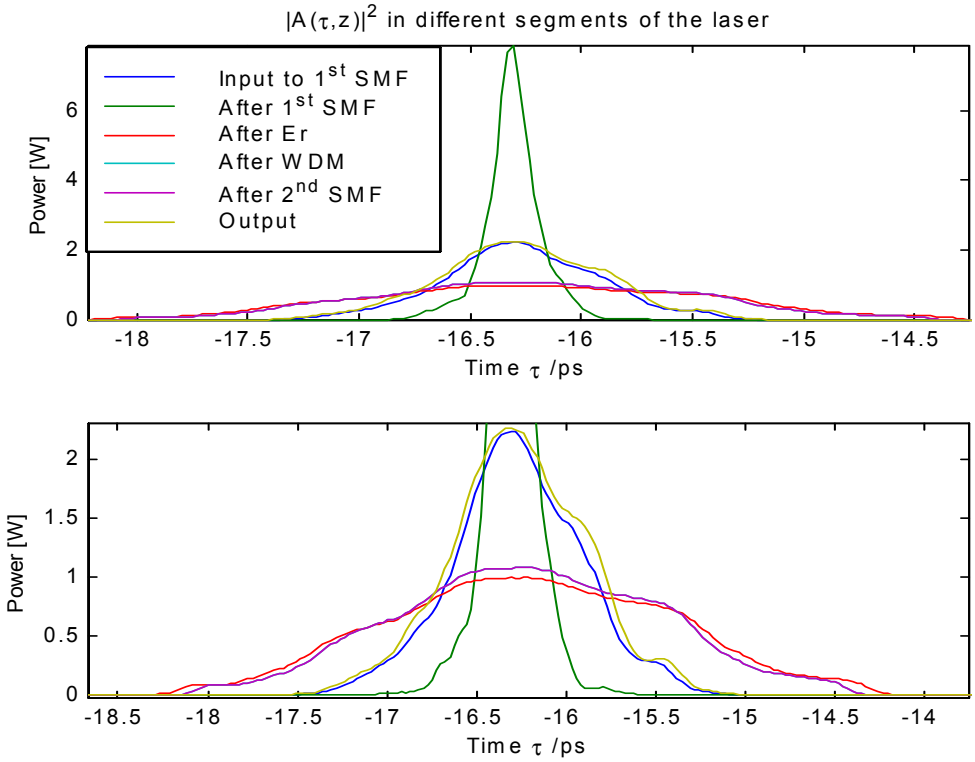

Figure 1.16.

Unfortunately these simulations were conducted after the real fibre ring laser was built and could not been used for the set-up. Perhaps these results can be used in the future considering the development in this area (all-fibre lasers). The program can be used for similar fibre-laser with some small changes and give a rough idea how a fibre laser will work. I think that the programs accuracy would have had improved if the Maxwell-Bloch equation were implemented into the program. As mentioned before, the limiting factor for this program is the factor T_2, dipole relaxation time, and when calculating the intra-cavity pulse width it is too close to its value. But that is outside the scoop of this dissertation. The results given will anyway serve as a foundation to stand on when designing a fibre ring laser.

2 Measurement of Group Velocity Dispersion

Introduction to Group Velocity Dispersion

For the fibre ring laser to generate stretched pulses the net dispersion of the cavity should be slightly positive, $D_T \approx 0.013$ ps^2. In order to know the correct fibre lengths it was necessary to measure the GVD of the fibres. Three different fibres are used in the laser, namely erbium doped fibre, Corning single mode fibre (SMF28) and a 980/1550 nm WDM fibre.

If an electromagnetic wave is incident on an optical medium it will interact with the bound electrons in the dielectric in different ways depended on the frequency of the wave and thus will travel a wavelength-dependent velocity. This effect is known as chromatic dispersion and is described by the refractive index, n(ω). As long as the electromagnetic frequency is far from any resonance frequency of the dielectric, the refractive index can be approximated by the Sellmeier equation:

$$n(\omega) = 1 + \sum_{j=1}^{m} \frac{B_j \omega_j^2}{\omega_j^2 - \omega^2} \ , \qquad (2.1)$$

where ω_j is the resonance frequency and B_j is the strength of the j th resonance. A higher frequency gives larger refractive index. It should be noted also that the spatial confinement, in a fibre, affects the refractive index and in turn contributes to the group velocity dispersion (GVD).
When a short optical pulse propagates through a fibre the different spectral components travel at different phase velocity given by c/n(ω) and group velocities given by ∂ω/∂k. Consequently the pulse increases its duration, because of its wide spectral width and of group velocity dispersion. This happens in any optical medium and needs to be taken into account when executing experiments.
The group velocity and GVD can be described in mathematical terms. Assuming that the frequency-dependent propagation factor β(ω) varies little within the bandwidth of the pulse, it can then be expanded in a Taylor series about the centre frequency ω_0 and is given by:

$$\beta(\omega) = n(\omega)\frac{\omega}{c} = \beta(\omega_0) + \frac{\partial \beta}{\partial \omega}(\omega - \omega_0) + \frac{1}{2!}\frac{\partial^2 \beta}{\partial \omega^2}(\omega - \omega_0)^2 + \ldots \ , \quad (2.2)$$

where the 1st derivative is the group velocity and defines the velocity of the pulse movement. The 2nd derivative is the group velocity dispersion (GVD) parameter. It shows that the pulse is broadened in time. The broadening arises because the individual spectral components travel with their own different group velocities. There are also higher order terms that can be included, but these are in general very small compared with the 1st and 2nd order terms.
When measuring group velocity, GVD and also 3rd order dispersion of short fibre lengths experimentally, equation (2.2) is used to calculate them. The only difference

is that it is done in the phase domain where phase is directly related to $\beta(\omega)$ because $\varphi(\omega)=\beta(\omega)\cdot L_{fibre}$. This relation will be derived bellow.

Experimental Configuration

One way of measuring GVD is to have kilometre long fibres and measure the pulse broadening in the time domain. Here, by using dispersive Fourier transform spectroscopy (DFTS) we can use shorter lengths, around 8 cm, to measure the GVD. A Michelson interferometer is used to obtain the interferograms at the output port. To be able to recover the interferograms it is necessary to have a low-coherence source. The coherence length for the source should be much shorter than the fibre used in the experiment. The interferogram is sensitive to the dispersion of each of the interferometer arms. By taking the Fourier transform of a single interferogram it's possible to extract the interferometric phase difference between the two arms of the interferometer across the spectral range of the source used.

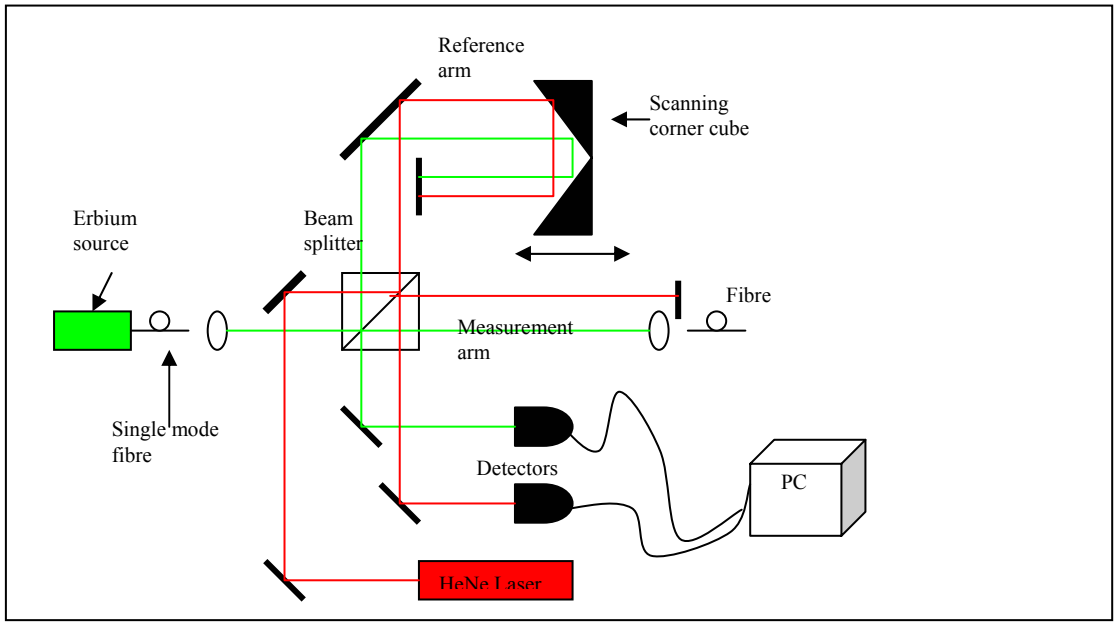

Figure 2.1.

The Erbium broadband source, from AMS Electronic GmbH with a bandwidth of 1527-1568 nm, is launched into the Michelson interferometer through a single mode fibre and a collimating microscope objective lens. The beamsplitter splits the beam in two parts, one of which continues into the measurement arm where the sample fibre is placed. Focusing into the fibre is also done with a microscope objective lens. Because of the shortness of the fibre there can appear cladding modes that will affect the interferograms, but by applying index matching gel on top of the fibre one can couple out the cladding modes and ensure single mode operation. A silica fibre of any sort has a facet reflectivity about 4%, which can be difficult to detect when using a low power source, so the end faces of the fibres were coated with a silver mirror, in a vacuum chamber by a thermal evaporation technique. The mirror thickness is around 30 nm and should correspond to 90% reflectivity. The enhanced reflectivity, from 4% to 90%, ensures ease of alignment from the back face of the fibre and good visibility

of the interferograms. The reference arm contains two mirrors and a corner cube that is mounted on top of a tilted granite rod. By launching compressed nitrogen into the corner cube mount, it can be floated and moves smoothly over the granite rod and can scan over a length of 1.5 metres. The total optical path length scanned is twice the fibre length times the refractive index. When scanning the reference arm over the required length a pair of interferograms is generated, due to reflections at the front and back faces of the fibre.
To assure accurate calibration of the scan when obtaining the generated interferograms a HeNe laser beam is launched parallel to the Erbium source. The wavelength of the HeNe laser is well known and has a well-defined coherence length, which makes it suitable for calibration. The HeNe used had a low coherence length of about 35 cm. The fibre length was chosen so that one scan could be done within the coherence length of the HeNe. Longer fibre lengths could be used but meant re-calibration of the HeNe and re-adjusting the length of the HeNe's measurement arm, to get the desired interferograms of both back and front faces. The HeNe fringes at the output port of the interferometer are detected with a high-speed silicon photo detector, with a 1mm^2 active area, and converted by an electronic circuit to TTL pulses. The TTL pulses are then used as a trigger at even intervals of group delay and are not affected by fluctuations in the scan speed. The output arm of the Erbium source is detected with an InGaAs photo detector, with a diameter of 80 µm from Hamamatsu, and sampled each time a "1" is given by a HeNe fringe, so that each sample corresponds to one wavelength of the HeNe, i.e. a resolution of 632.82 nm. The received data was collected through a data acquisition card in a PC with the software package LabView. The Fibre Group at Heriot-Watt University developed the program.

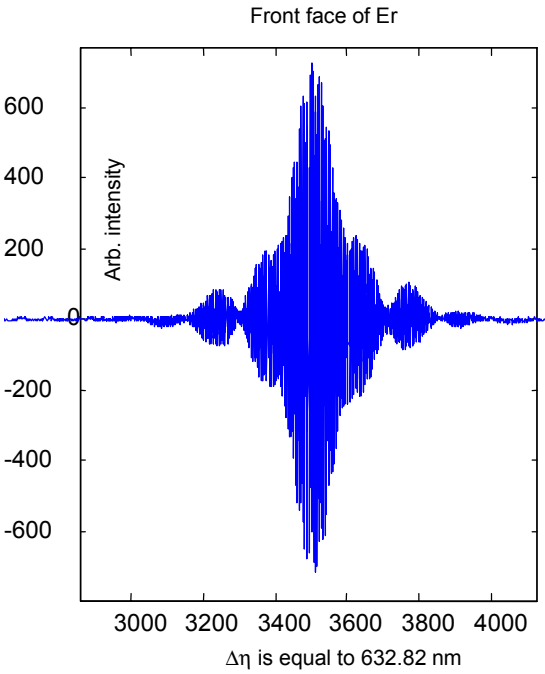

Figure 2.2.

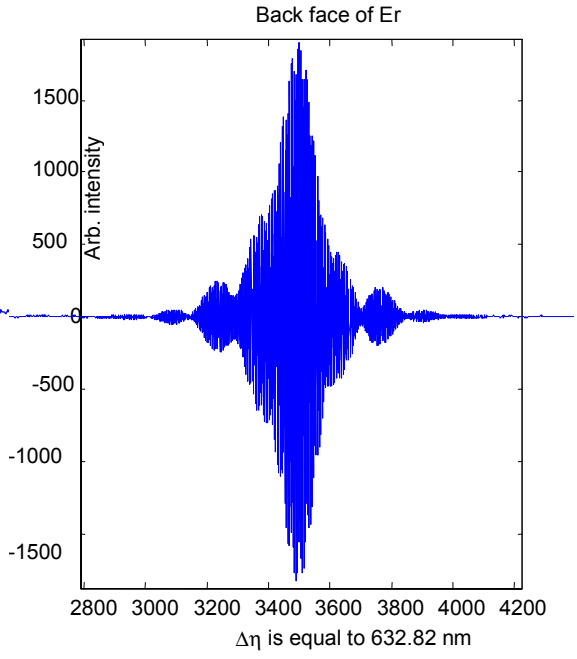

Figure 2.3.

The generated interferograms obtained from the front and back faces of the Er-doped fibre are shown in Figures 2.2 and 2.3. The front face data is relative symmetric around it's centre and contains the information about the dispersive phase of the

Michelson interferometer while the back face data is broader and is asymmetric around its centre. This is due to the dispersive nature of the fibre. Each window, i.e. Figure 2.2 and 2.3, has 7000 data points each spaced at 632.82 nm.
To understand how the group velocity, GVD and 3rd order dispersion is obtained from the interferograms a theoretical explanation will be given followed by a presentation of the measured data.

Theory

Considering that two electromagnetic fields interfere with each other at the output arm of the Michelson interferometer, the fields have low coherence so the interference is momentarily. The total intensity of the interference term is, $I(\tau)=\langle|E_1(t+\tau)+E_2(t)|^2\rangle$ and contains: two intensity terms related to the two fields in the arms, which when time averaged become a DC component (constants); and an oscillatory interference component that is a product of the two fields. τ denotes the relative time delay between the arms and brackets denotes time average:

$$I(\tau)=\frac{1}{\tau}\int_{t-\tau/2}^{t+\tau/2}\left|E_1(t+\tau)+E_2(t)\right|^2 dt, \tag{2.3}$$

The measured sample, in this case an optical fibre, is placed in the measurement arm in the Michelson interferometer, and acts as the dispersive element in that arm. The intensity at the interferometer output arm can be written as a function of τ, [14]:

$$\mathrm{I}(\tau)=\mathrm{I}_0+\mathrm{I}_{os}(\tau), \tag{2.4}$$

where I_0 denotes the sum of the DC components and $I_{os}(\tau)$ is the oscillatory component, which contains the phase information. $I_{os}(\tau)$ is proportional to the real part of the mutual coherence function $\Gamma_{12}(\tau)$, which can be seen from equation (2.3), given by:

$$\Gamma_{12}(\tau)=\left\langle E_1(t+\tau),E_2(t)\right\rangle, \tag{2.5}$$

where $E_m(t)$ is defined at a distance z from the beam splitter in arm m as:

$$E_m(t)=\int_{-\infty}^{\infty}\widetilde{E}_m(z,\omega)\exp\{i\phi_m(\omega)\}\cdot\exp\{-i\omega t\}d\omega \quad m=1,2, \tag{2.6}$$

where $E_m(z,\omega)$ is the Fourier transform of the field $E_m(z,t)$ and $\phi_m(\omega)$ is the dispersive phase function. Normalising equation (2.5) and using equation (2.6) in the same, the exp(-iωt) term in $E_m(t)$ respectively cancels out because of the complex conjugate in equation (2.5).

The "new" mutual coherence function can be written as:

$$\gamma_{12}(\tau) = \int \widetilde{G}(\omega) \exp\{-i[\phi_1(\omega) - \phi(\omega)]\} \cdot \exp\{i\omega\tau\} d\omega, \tag{2.7}$$

where

$$\widetilde{G}(\omega) = \frac{E_1^*(\omega) E_2(\omega)}{\sqrt{\Gamma_{11}(0)\Gamma_{22}(0)}}, \tag{2.8}$$

is the normalised spectral distribution function of the source. Using the previously mentioned relations one can conclude the following:

$$I_{os}(\tau) \propto \mathrm{Re}[\gamma_{12}(\tau)], \tag{2.9}$$

and

$$\gamma_{12}(\tau) = F^{-1}\left[\widetilde{G}(\omega) \exp\{-i[\phi_1(\omega) - \phi_2(\omega)]\}\right] = F^{-1}\{S(\omega)\}, \tag{2.10}$$

Taking advantage of the linearity of Fourier transform and expanding the real part of γ_{12} and assuming that complex spectrum, $S(\omega)$, is zero for negative values of ω it gives $S(\omega)=F\{2Re[\gamma_{12}(\tau)]\}$, combining it with equation (9) gives:

$$\begin{aligned} &\widetilde{G}(\omega) \exp\{-i[\phi_1(\omega) - \phi_2(\omega)]\} \propto F\{I_{os}(\tau)\}, \\ &\widetilde{G}(\omega) \propto \left|F\{I_{os}(\tau)\}\right|, \end{aligned} \tag{2.11, 2.12}$$

and

$$\varphi(\omega) = \arg F\{I_{os}(\tau)\}, \tag{2.13}$$

where equation (2.13) gives the dispersive phase of the system, which is only the argument of the Fourier transform of the oscillating intensity component, i.e. the interferogram. Equation (2.12) gives the normalised amplitude spectrum. To measure the group velocity and the GVD parameters of a fibre, two measurements need to be done. First of all, we measure the dispersive phase for the Michelson interferometer, which is recovered from the front face data. Then we measure the dispersive phase recovered from the back face data, which now contains the dispersive phase of the interferometer and the fibre. To extract the dispersive phase for the fibre we simply subtract the two measured dispersive phases from each other, i.e. $\varphi_{fibre}(\omega)=\varphi_{back}(\omega)-\varphi_{front}(\omega)$.

While expanding φ(ω) in a Taylor series around a centre frequency ω_0:

$$\varphi(\omega) = \varphi(\omega_0) + \frac{\partial\varphi}{\partial\omega}(\omega-\omega_0) + \frac{1}{2!}\frac{\partial^2\varphi}{\partial\omega^2}(\omega-\omega_0)^2 + \frac{1}{3!}\frac{\partial^3\varphi}{\partial\omega^3}(\omega-\omega_0)^3 + \ldots, \quad (2.14)$$

The easiest way would be to numerically differentiate the phase curve φ_{fibre}, but the noisy character of the curve would not allow this, so a polynomial fit to φ_{fibre} was done. From there the group velocity, GVD and even 3rd order dispersion can be extracted, according to equation (2.14).

Dispersion Measurements on SMF28, Er-doped and WDM Fibres

Four different fibres were dispersion characterised, the lengths of the fibres were: SMF28 l_{smf28} = 76.1±0.1 mm, Er-doped (highly doped) DF1500L from Fiber Core ltd. l_{Er1} = 86.0±0.05, Er-doped DF1500L from Fiber Core ltd. l_{Er2} = 81.8±0.05 mm and a WDM fibre l_{WDM} = 84.2±0.05 mm. The length could also be calculated from the spacing between the front and back interferograms, but the only known refractive index was for the single mode fibre, n = 1.46, the calculated length became then 76.2 mm for the SMF28, which corresponded well to the measured length.
After recovering the interferograms from the Michelson interferometer on the computer and saving them as binary data they were processed and analysed with the software package MatLab. The program used was mainly written by the fibre group but modified for this analysis. The steps in analysing the interferograms are straightforward. The interferograms are windowed so that the top peak is centred, see Figure 2.2 and 2.3, and the window chosen to be as large as possible. Here η = 7000 sampled data points were chosen, but for processing with fast Fourier transforms in MatLab numbers of point should be chosen to a power of 2, i.e. 2^n. But the interferograms of the front face of the fibre and the focusing lens were too close to achieve this while maintaining a sufficient large window. This does not affect the analysis but just slows it down.

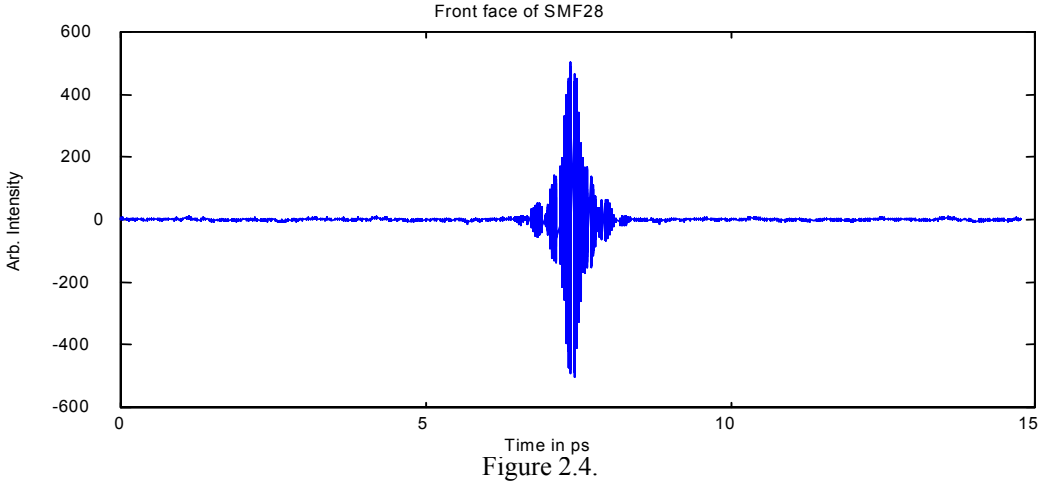

Figure 2.4.

Knowing the spacing within the interferogram, $\Delta\eta = 632.82$ nm, it is easily converted into a time base by dividing HeNe wavelength with the speed of light. See Figure 2.4. The peak of the interferogram corresponds to the point where zero optical path difference occurs between the arms of the Michelson interferometer.
The step size in time becomes then $\Delta\tau = 2.11$ fs, which corresponds to one HeNe fringe, and the whole window size is $T = \eta * \Delta\tau = 15$ ps. Applying the discrete Fourier transform to the interferogram, this gives in the Fourier domain the inverse relation, i.e. $\Delta f = 1/T$ and $F = 1/\Delta\tau$. And by stepping up with Δf in the frequency plan from 0 up to F gives the real calibrated spectrum.

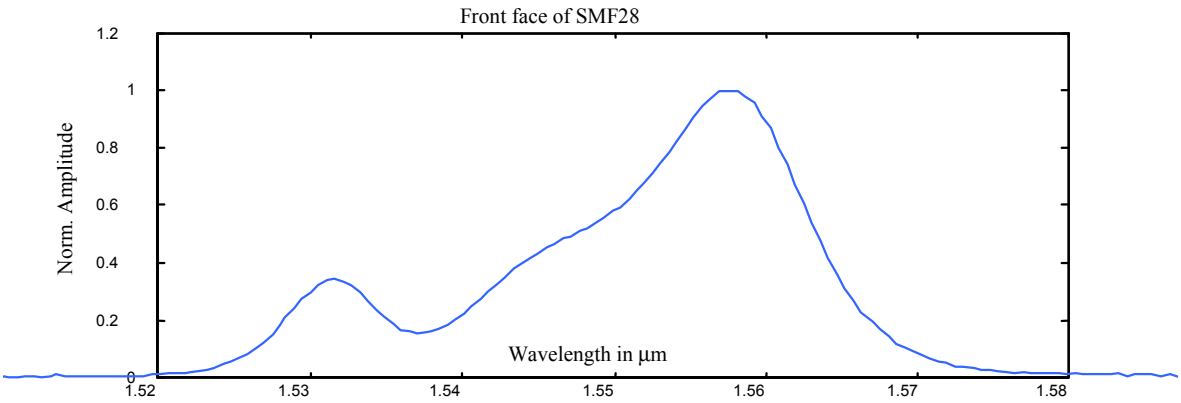

Figure 2.5.

As seen in Figure 2.5, with equation (2.12) the amplitude spectrum of the Erbium broadband source can be shown and is plotted vs. wavelengths. It corresponds to the specifications given by the manufacturer of the Erbium source. The argument of the Fourier transform of the normalised mutual coherence function, *S(ω)*, were phase-unwrapped, which removes the 2π discontinuities, to obtain a phase curve $\varphi(\omega)$, i.e. equation (2.13).

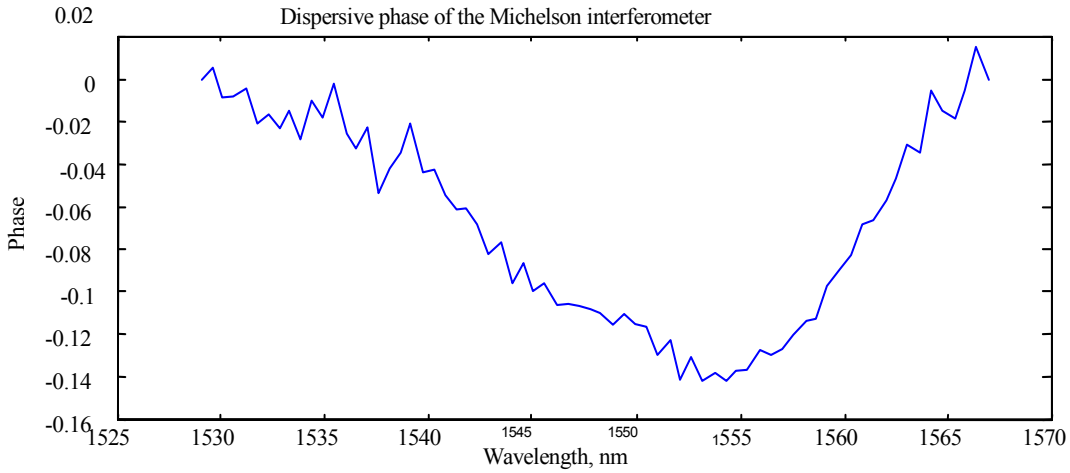

Figure 2.6

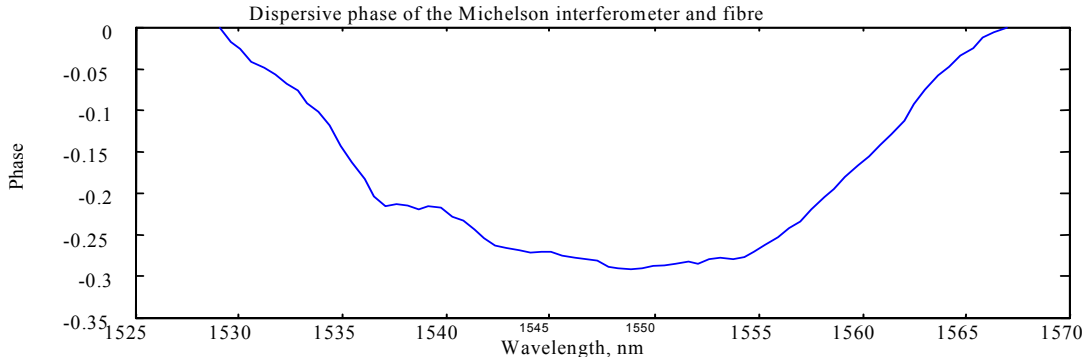

Figure 2.7.

Figure 2.6 and 2.7 shows the dispersive phase of the Michelson interferometer (front faces) and interferometer with fibre (back faces), respectively. In Figure 2.6, the difference in phase is mainly due to the microscope lens in the measurement arm and beamsplitter. Other effects such as air currents and temperature fluctuations over the arms in the interferometer are negligible. The noisy character of the front face, Figure 2.6, is because only 4% is reflected and thus gives a lower signal-to-noise ratio than the back face which has a reflectivity of ~90%. Extracting the dispersive phase for the fibre is done with the relation, $\varphi_{fibre}(\omega)=\varphi_{back}(\omega)-\varphi_{front}(\omega)$. See Figure 2.8.

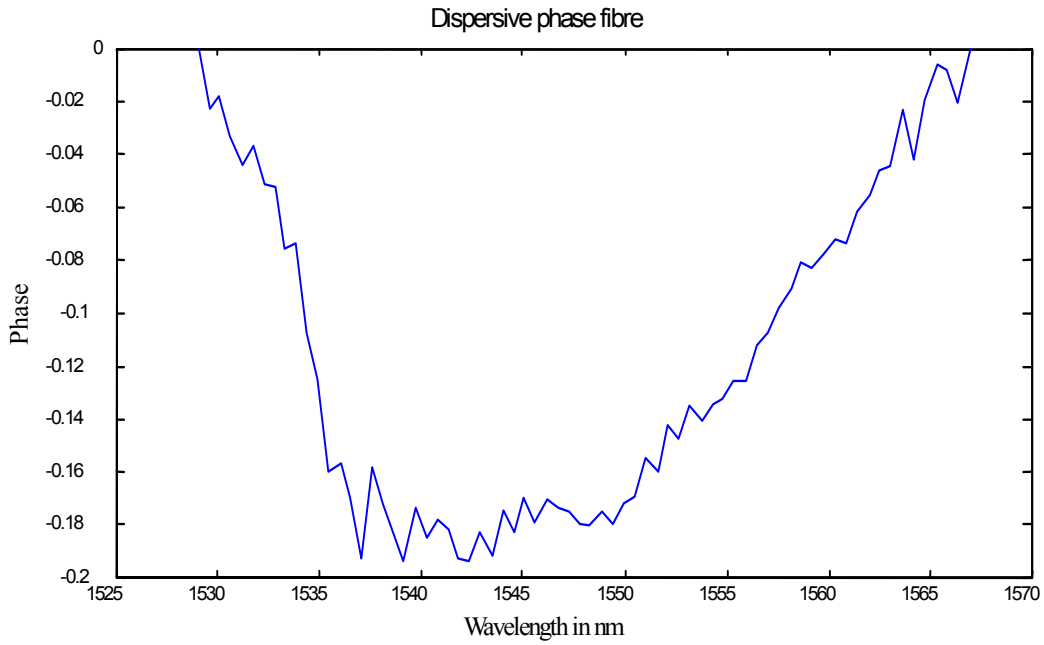

Figure 2.8.

Finally, over the given frequency range, pictured here in wavelength, a MatLab command that produce a 2nd order polynomial fit to the unwrapped phase and the program calculates the coefficients to the Taylor series shown in equation (2.14). As evidenced by the fit residuals of Figure 2.9, a 3rd order fit would give a significant improvement in the accuracy of phase estimation, indicating that 2nd order dispersion was present.

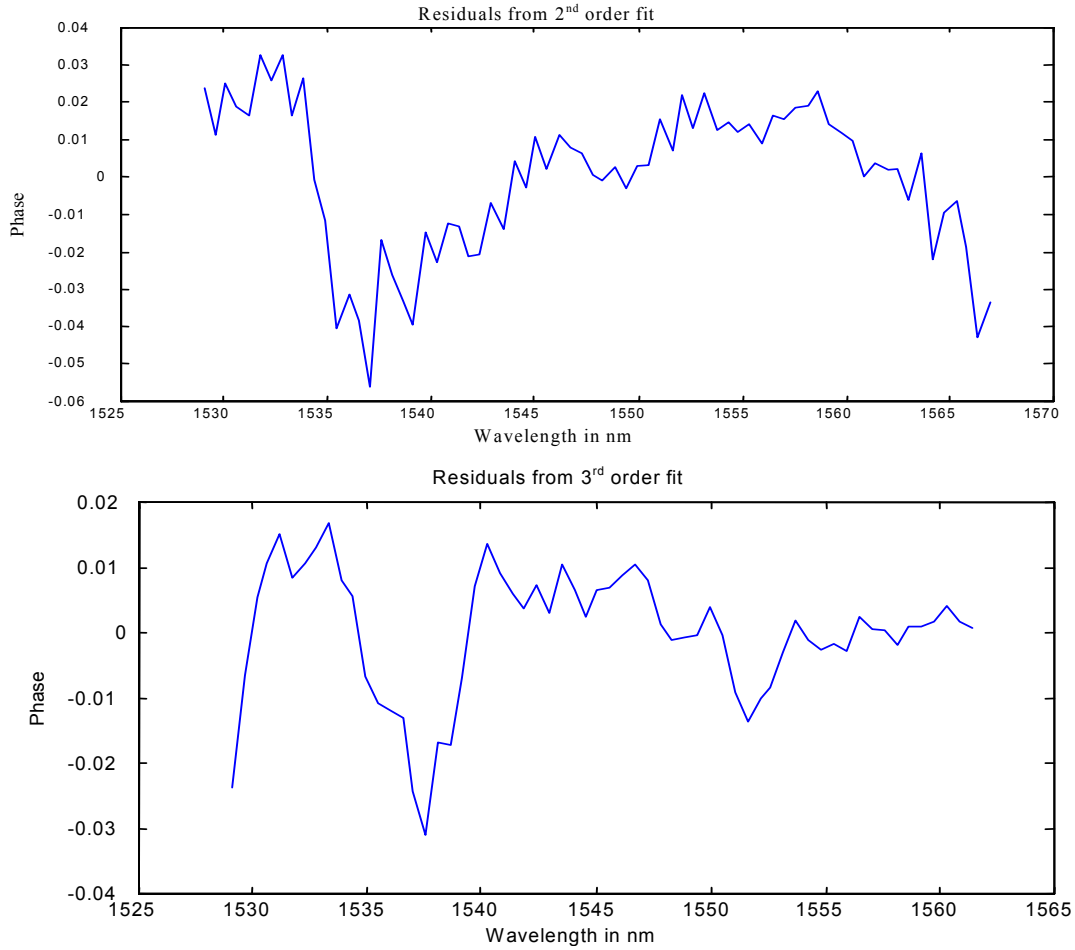

Figure 2.9 & 2.10.

The fit residuals of the 3rd order, Figure 2.10, are mainly due to noise in the interferograms and higher order polynomial fits gave no further measurable reduction in the fit residual. Thus higher order dispersion was negligible and a 3rd order fit was applied in all cases.

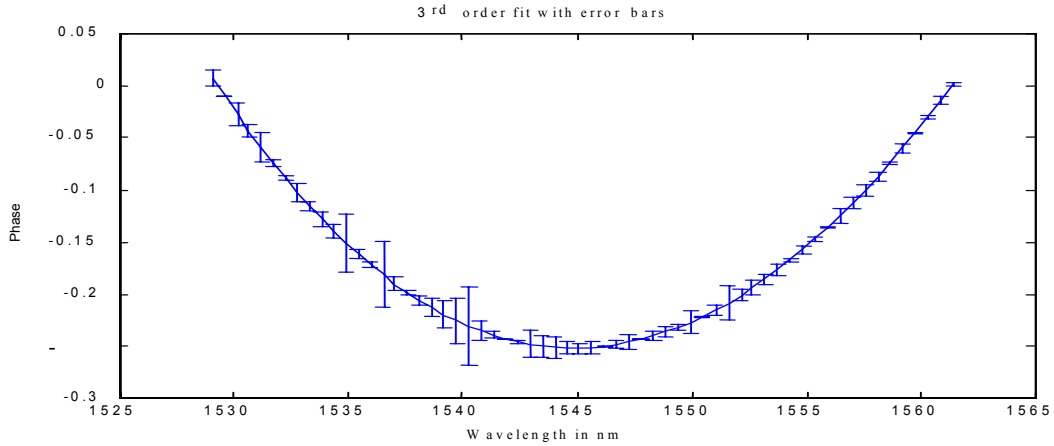

Figure 2.11.

With a 3rd order fit the discrepancy from the measured data is small, shown here with error bars in Figure 2.11. Twenty measurements were done on each fibre, ten with index matching gel and ten without; one measurement contains two interferograms, front and back faces. The dispersive phase for the fibres was calculated as mentioned above. After the polynomial fit was done for each individual measurement, an average was taken over the second-order coefficients and divided by the length of the measured fibre in order to give the GVD coefficients.

Results

To check the accuracy of the measurement technique, a SMF28 was measured, which has a well-known GVD (-23ps^2/km @ 1550 nm) parameter.
The measured GVD became with index matching gel:

$$-(22.75 \pm 0.91)\ \text{ps}^2/\text{km} @ 1545\ \text{nm}$$

without index matching gel:

$$-(21.63 \pm 1.16)\ \text{ps}^2/\text{km} @ 1545\ \text{nm}.$$

The presence of cladding modes is the probable cause of the difference in the measured GVD parameters. The measured dispersion agreed well with the known dispersion for the SMF28. Further calculations should be accurate as well. The standard deviation in the final GVD measurements is calculated as follows, [15]:

$$\left(\frac{\Delta\beta_2}{\beta_2}\right)^2 = \left(\frac{\Delta L_{fibre}}{L_{fibre}}\right)^2 + \left(\frac{\Delta\varphi^{(2)}}{\varphi^{(2)}}\right)^2, \qquad (2.15)$$

β_2 is the GVD, $\varphi^{(2)}$ is second-order polynomial coefficient, L_{fibre} is the fibre length and the Δs is the standard deviations, respectively.
The standard deviation for the fibre lengths is due to the resolution of the ruler used and for $\varphi^{(2)}$ it is calculated from the ten different measurements.
The following calculated results were obtained:

Fibre	Length (mm)	@ wavelength (nm)	GVD (ps^2/km)
Er-doped fibre Highly doped:	86.0±0.10	1547	+23.51±0.21
Er-doped fibre	81.8±0.10	1547	+20.28±0.46
WDM fibre	84.2±0.10	1548	-9.94±0.18
SMF28 fibre	76.1±0.10	1545	-22.75±0.91

Table 2.1.

The length of the fibres in the ring laser was cut according to these calculated GVD parameters, to achieve a positive net dispersion of the cavity of ~0.013 ps^2. The results depicted in Table 2.1 are for the fibres measured with index matching gel. Other sources of error can be that the dispersion of air is not taken into account in the calculations, other limitations, such as the detector response when detecting the fringes and fluctuations in nitrogen pressure that would give vibrations in the reference arm and could degrade the interferograms. These errors are not included in the standard deviation in Table 2.1.
To increase the signal-to-noise ratio for the front face interferogram, a filter in front of detector would do and thereby would be able to increase the launch power of the Erbium broadband source into the system. The added dispersion from the filter would not effect the measurements, because only the relative difference is calculated.

3 Experimental Set Up

Splicing of the Fibres

Before any laser operation is conducted, the different fibres must be spliced together. Prior to splicing you need to strip off the coating, clean and cleave the fibres. This was performed with a “stripper” and a mechanical cleaver.
The fibres used in the ring laser have different core radii, which means when splicing, it is crucial that the cores are well centred and aligned with each other. This was accomplished with an automatic fusion splicer. The fusion splicer discharges an arc of high voltage over the fibre to burn away residue dust so that the cleaved fibre ends are perfectly cleaned. On a screen connected to the fusion splicer it was possible to confirm that the cleave and splice was adequately done. The splicer then aligns the individual fibre cores and voltage is applied over the fibres so that they “melt” together. Even though this procedure is very precise there will be losses, because of core-radius mismatch and differences in refractive index. The fusion splicer measures the loss perpendicular to the splicing direction and gives a rough idea of the losses. Losses less than 0.03 dB were sufficient. The equipment used for cleaving, “stripping” and splicing the fibres was borrowed from the Fibre Group at Heriot Watt University.
There are different ways to protect the spliced fibres, one way is to deposit a protecting jacket over it or place it on cardboard and hold it down with tape. If the probability of re-splicing is high, then cardboard protection is preferred, because the loss of fibre length is a minimum. In configuring the laser for mode locked operation the role of the different fibres is important and the measurement of their dispersion has already been described in the previous section.

Set Up

The ring cavity contains of 2.02 m highly Er-doped fibre from Fibre Core Ltd., 1.36 m of SMF-28 (single mode Corning fibre), 0.42 m of 980/1550 nm WDM coupler, a bulk isolator, a birefringent plate (BFP) and polarising beam splitter (PBS). Instead of using bulk waveplates like in [17], we use polarisation controllers (P-controllers) that are made out of SMF28 around circular holders; one or two revolutions are equal to a quarter and half wave plate, respectively. The bulk isolator is a Faraday-Rotator with two polarising sheets. The sheets are tiled of an angle of 45^{o} degrees to each other, which then assures unidirectional lasing.
A pump laser diode from Marconi Caswell Ltd was used that had a maximum average output power of 430 mW @ 980 nm when a drive current of 500 mA was applied. The pump was mounted on a translation stage with x-, y- and z-actuators. The pump light was then collimated with an aspherical lens, f = 2.93 mm; NA = 0.4, and then focused into the WDM coupler with a focusing lens (aspherical), f = 2.8; NA = 0.4, thus a demagnification occurs. The WDM fibre was also mounted on a 3-D translation stage for “easy” focusing. The measured NA for the WDM fibre coupler was ~0.15. Coupling to free space is achieved using fibre pigtailed lenses, which were mounted on specifically designed fibre lens holders. The PBS, isolator and BFP were mounted

on posts for ease of alignment (see Figure 3.1.). Usually the BFP is used at Brewster's angle, but the fibre pigtailed lenses did not give a well collimated beam over a large distance, keeping the free space region as short as possible was necessary. However, with the beam incident perpendicular to the BFP, the laser did not lose much of it output powers. At first it actually increased because the polarising

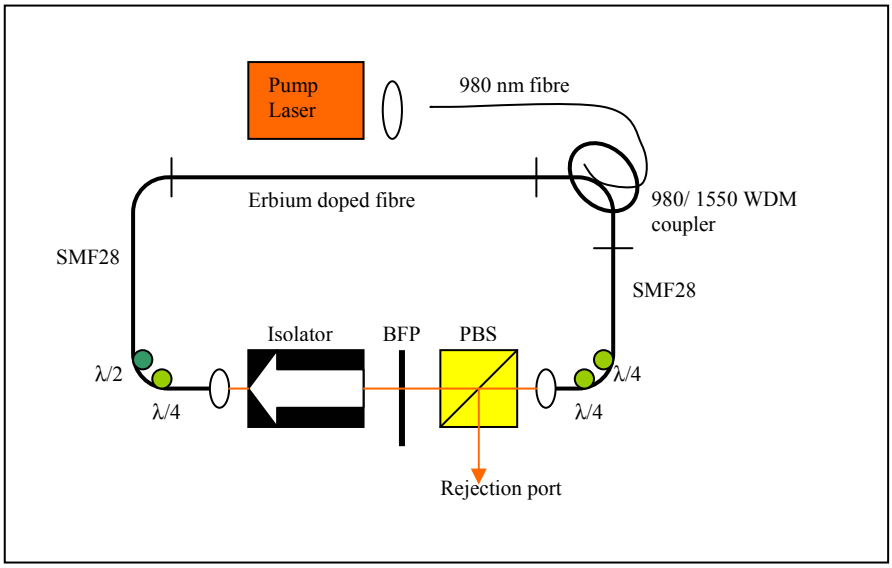

Figure 3.1.

sheet in the isolator wasn't aligned with the polarisation direction of the PBS. By rotating the BFP it was possible to set the polarisation direction of the light beam so that it coincided with the polarisation sheet of the isolator. As can be seen in Figure 3.1, the laser was backward pumped, which meant that the 980 nm pump light propagated in the opposite direction to the lasing 1530 nm. In physical terms, the fibre amplifies a signal as erbium atoms absorb the pump radiation and transfer their energy to the signal, and the intensity of the pump radiation decreases over the length of the fibre. As the clockwise propagating signal (1530 nm) travels through the erbium fibre, its intensity increases and encounters higher gain further down the fibre. To get effective amplification it is necessary to have sufficient pump power so that the signal does not get absorbed in the beginning of the Erbium-doped fibre. By looking at the excited state absorption of the Erbium, that emits green light, it was feasible to empirically determine whether or not sufficient pump power was launched.

Coupling Efficiency

The pump laser diode from Marconi Caswell Ltd. were kept on a Peltier cooler at 14^{o} Celsius for effective performance, the temperature dependence of the emitting spectrum is unknown. Two diode designs were used and the emitting surface has two different widths, 6 µm and 9 µm. The 980 nm single mode fibre connected to the WDM coupler had a modal field diameter of 6.6 µm, so the 6 µm devices were chosen for the best coupling efficiency. The difference in NA between the WDM fibre and the focusing lens makes the coupling from the laser diode into the fibre poor.

Another major contributing factor for the low coupling efficiency was that the beam quality of the laser diode worsened when increased drive current was applied. The beam changed its spatial mode remarkably, which in turn meant a lot of effort going into refocusing the launched pump light into the WDM fibre. A maximum coupling efficiency of 45 % was reached at a drive current of 250 mA and kept there until the drive current reached 450 mA. This was understood as

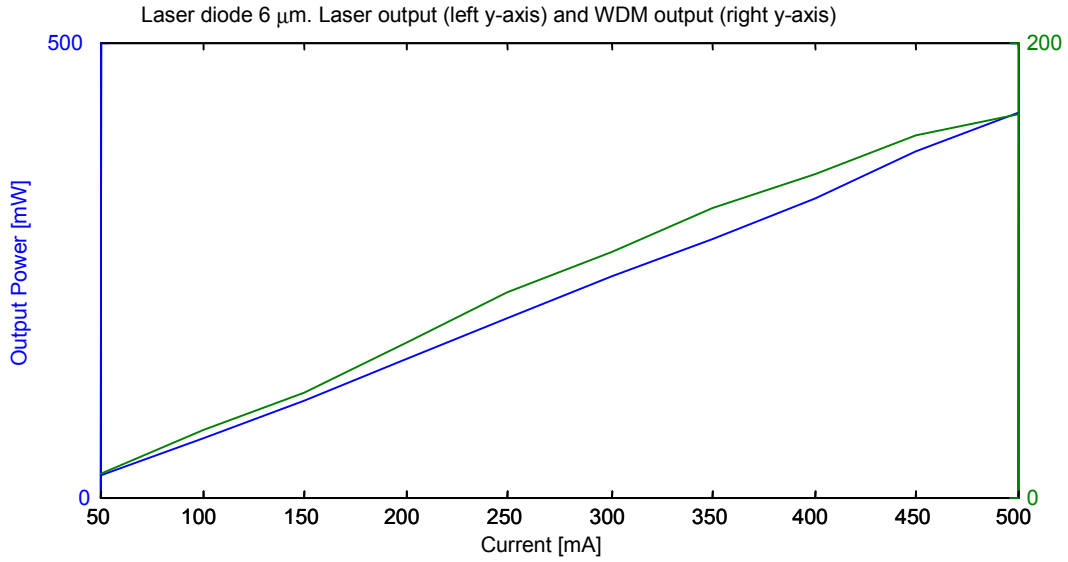

Figure 3.2.

an increase in the spatial mode size which was not confined within the 6 μm width, hence, the coupling efficiency dropped. The performance of the different devices (pump lasers) varied a lot, and measurement of the coupling efficiency was made on one device that broke. The currently used pump laser had better over all performance and the results are shown in Figure 3.2. It should be noted that we measured the output at the rejection port of the laser and were interpolated with previously made measurements at the output of the WDM coupler. The changes in spatial modes were random and highly dependent on the temperature and applied drive current. Even though these difficulties and low coupling efficiency, the launched power into the Er-doped fibre for maximum drive current (500 mA) had an average value of 180 mW, which should be sufficient for mode locking.

980 nm Absorption

When looking at the operational wavelength of the pump laser diode it was noted that not only the spatial mode shifted but also the spectrum varied over a range of 15 nm. Figures 3.3a and 3.3b show the spectrum for the pump laser, they are shown for different drive currents, 200mA and 450 mA, respectively. The spectrum was measured with an *ist-rees Laser Spectrum Analyzer* and viewed on a *Tektronix TDS3032 real-time digital oscilloscope*. The temperature for the both measurements was kept the same. The broadening in the spectrum can have its origin from over population of electrons in the well-defined energy levels in the quantum well structure of the pump laser. Thus, when higher drive current is applied, for example, the first energy level becomes full and a broadening of the state take place, so when electrons

fall down to the ground state a broadening of the spectrum occurs. Even higher energy levels will be populated and emit photons

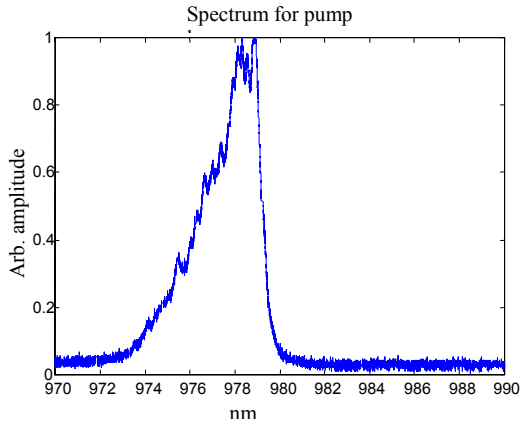

Figure 3.3a.

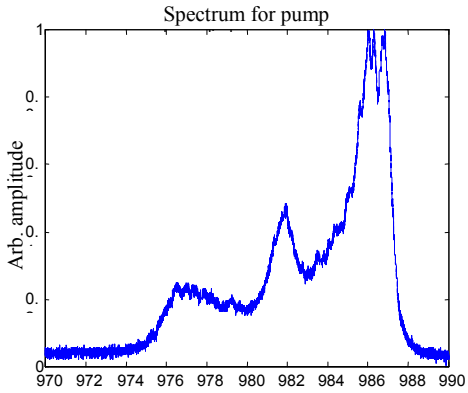

Figure 3.3b.

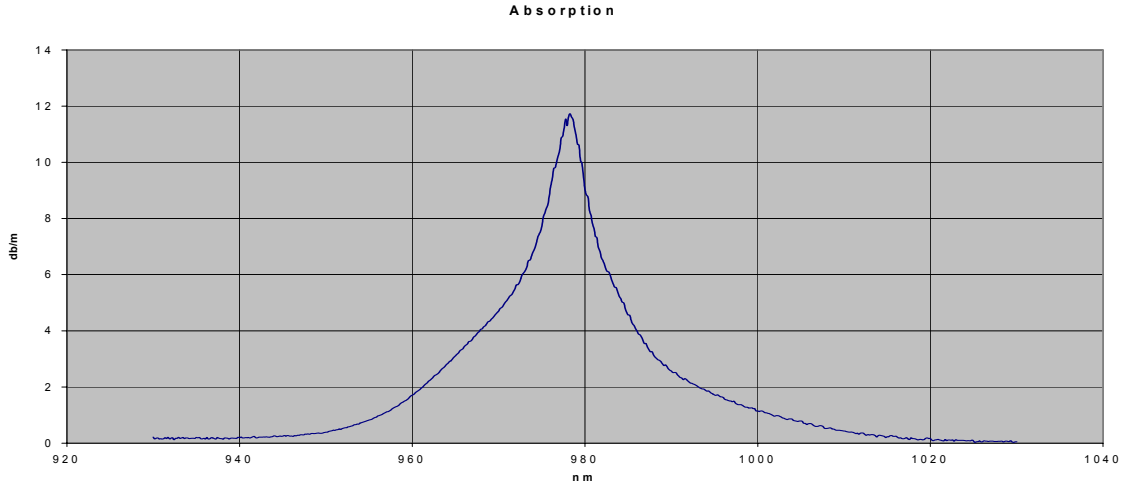

Figure 3.4. (Courtesy of Fibre Core Ltd.)

according to their defined energy level. However, the broadening of the pump laser spectrum doesn't affect the excitation of Erbium ions noticeable. This Erbium-doped fibre has it maximum peak absorption around 11.8 dB/m @ 978 nm and has a broad absorption spectrum around it, seen in Figure 3.4. The broadness can be explained as follows. In a glass host (here silica fibre), erbium ions are subjected to electric fields, known as crystal fields due to the surrounding atoms in the host lattice. This causes Stark splitting of the erbium ion orbitals, and dependent where the erbium ions are located in the glass host the ions encounter variations of the field due to the amorphous structure of the glass. Resulting in an inhomogeneous broadening of the transition. Other effects are phonon broadening (homogeneous broadening) that is temperature-dependent [18].

Short Theory

In this part a short presentation of mode locking in general and mode locking in the fibre ring laser will be conducted. The more extensive theory of the physical

mechanism behind the fibre ring laser has been given in the first section where the numerical modelling is also described.

General Mode Locking Theory

Without mode locking, all the modes oscillate independently of one another with random phases, thus giving continuous wave (CW) operation. To explain mode locking in a simple way, consider the frequency spacing among modes in a CW laser, which is given by:

$$\Delta\nu = \frac{c}{L_{optical}}, \tag{3.1}$$

where $L_{Optical}$ is the optical path length of one round trip inside the cavity. For the FRL used in this report $L_{Optical} = n_{eff}L_{fibre}+L_{space}$, where n_{eff} is the effective mode index, L_{fibre} is the fibre length and L_{space} is the free space length and optical isolator path length. Within the gain profile of the Er-doped fibre thousands of modes can be sustained and closely spaced modes can reach threshold simultaneously and encounter the same gain. The summation of all the modes can be written mathematically as:

$$E(t) = \sum_{m=-k}^{k} E_m \exp(i\varphi_m - i\omega_m t), \tag{3.2}$$

where E_m, φ_m and ω_m are the amplitude, the phase and the frequency of m^{th} mode, respectively. When the phases of different frequency modes of a laser are independent, the summation term becomes time independent and the laser is CW with multiple modes. However, with the mode locked laser, all the cavity modes are forced to be in phase at one point within the cavity. The phase difference between two adjacent longitudinal modes is locked to a constant value φ i.e.

$$\varphi_m - \varphi_{m-1} = \varphi, \tag{3.3}$$

From equation (3.3) it is easily seen that $\varphi_m = m\varphi + \varphi_0$ and that mode frequency can be written as $\omega_m = \omega_0 + 2m\pi\Delta\nu$.
Using the new parameters in equation (3.2) and execute the summation, with the assumption that all modes have same amplitude E_0, the intensity then becomes:

$$\left|E(t)\right| = \frac{Sin^2\left[(2M+1)\pi\cdot\Delta\nu\cdot t + \frac{\varphi}{2}\right]}{Sin^2\left[\pi\cdot\Delta\nu\cdot t + \frac{\varphi}{2}\right]} E_0^2, \tag{3.4}$$

The result is a laser output with regularly spaced pulses and such “mode locked” lasers usually produce trains of pulses with durations of a few ns to fs (true for passive mode locking) resulting in high peak powers. The pulse repetition rate is the frequency mode spacing $\Delta\nu$, thus the spacing among pulses are $\tau_r = 1/\Delta\nu$.

Mode Locking Mechanism in the Fibre Ring Laser

The optical isolator plays a double role in the sense that as an isolator it gives unidirectional laser oscillation, and also linearly polarises the light leaving it. This FRL is back-pumped, so when launching the 980 nm light into the WDM coupler the isolator absorbs the residual 980 nm that leaves the Er-doped fibre.
Before the light reaches free space it goes through the P-controllers, the first of which changes the polarisation to circular. The different polarisation states then propagate non-linearly through the fibre, mostly due to the Kerr effect. The Kerr effect is intensity dependent, thus, higher intensity leads to a greater induced phase shift between the orthogonal polarised states. To get the intense part of the light through the polarisation sensitive isolator the second polarisation controller needs to be set in a proper way. The most intense part of the light is then transmitted into the cavity for another round trip and the low intensity field is coupled out through the rejection port. By suitably adjusting the P-controllers in the fibre ring laser it will work as a fast saturable absorber. Another non-linear effect is self-phase modulation (SPM), which causes spectral broadening. SPM is dominant under pulse operation but it also affects the oscillation under CW regime. In the CW regime, partially coherent light exhibits both intensity and phase fluctuations. SPM converts intensity fluctuations into additional phase fluctuations and broadens the optical spectrum. These perturbations (spikes) in the intensity and in the spectrum generate new frequencies and leads to the "signature" for mode locking. This is the mechanism for the polarisation additive-pulse mode locking (P-APM). The other two polarisation controllers are to give stability and the right polarisation state to the output arm, [6]. The fibres used are very sensitive to bending, which changes the polarisation states of the propagating light. This can be used to help the fibre ring laser to mode lock, even a light touch changes the polarisation.

Dispersion

At the rejection port "stretched" pulses will be generated. To stretch the pulse temporally the net dispersion in the cavity needs to be positive. The fibre ring laser consists of two sections, one with positive group velocity dispersion (GVD) (the Er-doped fibre) and one with negative GVD (the SMF28 and the WDM fibre). The net dispersion of the two sections is almost balanced and close to zero, but positive. The mode locked pulse stretches and compresses as it propagates around the cavity, see Figure 1.15 and 1.16. The target net dispersion for our configuration is about + 0.013 ps^2 and would ensure a positive chirp. The well-known GVD parameter for SMF28 is – 23 ps^2/km and the measured GVD parameter for the Erbium doped fibre was + 23.5 ps^2/km and for the WDM fibre it was – 9.4 ps^2/km. The measurement technique and the theory on GVD were discussed in the previous section. The reason for having a positive net dispersion is to lower the peak power resonant in the fibre, so that non-linear effects decrease which in turn avoids saturation of the APM action. Because of this, it is possible to generate high-energy, broad bandwidth pulses, [4].

Laser Operation

As mentioned before it was critical to have as short free space region as possible, and this meant constructing mounts to hold the bulk components in an efficient way. Different kinds of set-ups were conducted, and the lengths of fibres and the free space region were continuously changed before settling for the configuration shown in Figure 3.1. Pumping the erbium with 980 nm we first recorded the fluorescence spectrum of the erbium shown in Figure 3.4, it corresponds well with the gain spectrum given by Fiber Core Ltd. Finally everything was in place and after aligning the free space section the laser oscillated. The threshold for laser oscillation was 11 mW of launched pump power giving a maximum output power at the rejection port of 4 mW. In Figure 3.5 the spectrum of the fibre ring laser at a launched pump power of ~100 mW is shown.

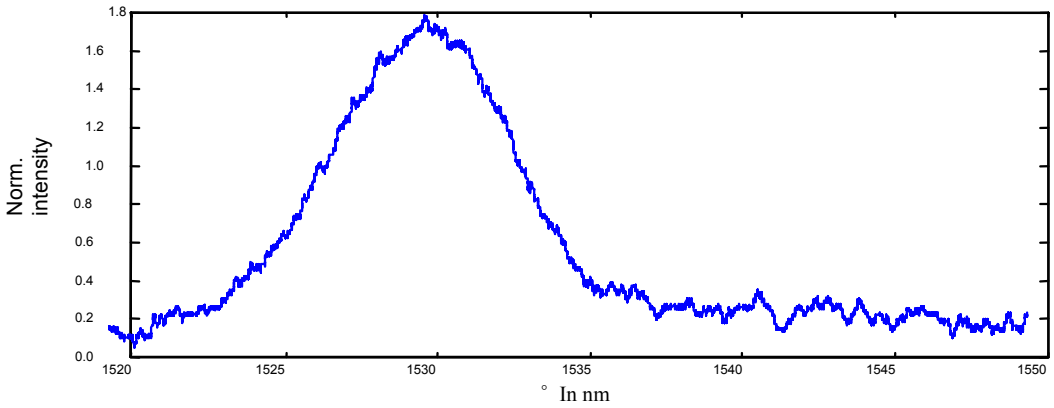

Figure 3.4.

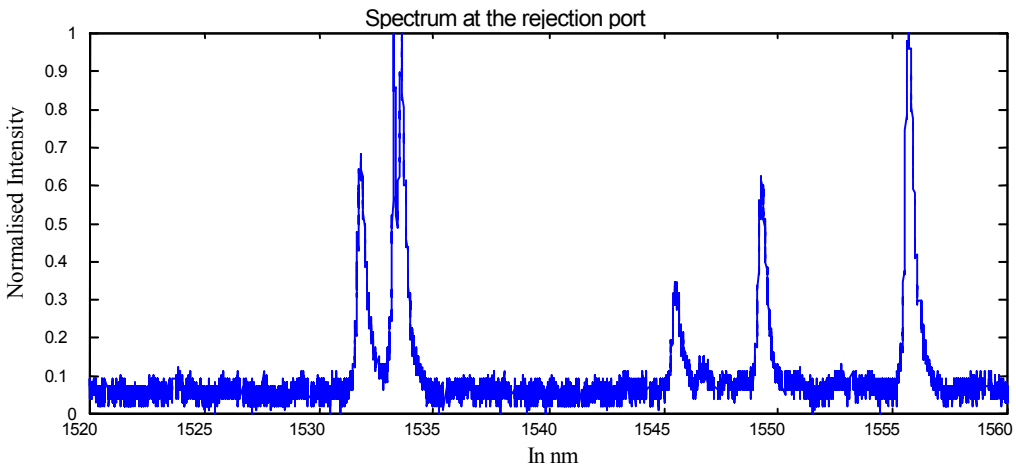

Figure 3.5.

The corresponding maximum output power was 30 mW. Tuning of the spectrum was achieved with the BFP and the polarisation controllers and could be easily tuned over the whole gain spectrum of the Erbium-doped fibre. However, not without mode hops. When changing the settings of the BFP and the P-controllers the output power at the rejection port changed by up to an order of magnitude. The slope efficiency curve of the laser output vs. pump power is shown in Figure 3.6 for the setting with the highest output powers. The CW output power at maximum pump power is relatively high compared with other reports on all-fibre laser systems seen in [16] and

[17]. Even though the set-ups differ a little bit the overall performance looks promising for mode-locked operation.

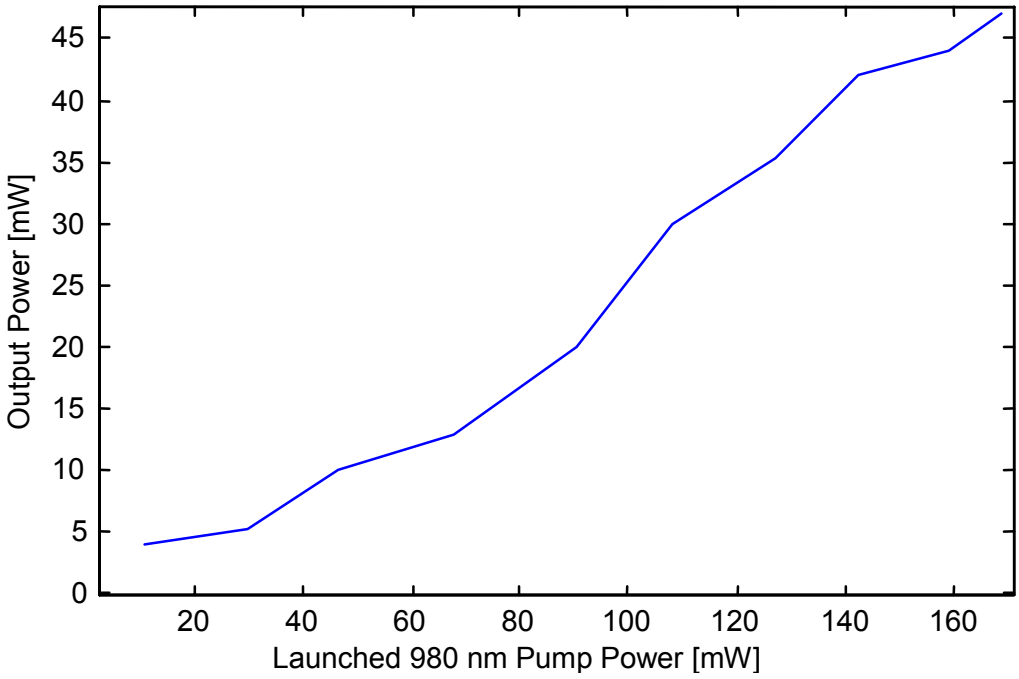

Figure 3.6.

Trying to achieve mode locking in the APM laser, one must first of all maximise the output power at the rejection port in the CW regime. Then by looking at the frequency spectrum in real time one maximises the numbers of CW-spikes by adjusting the P-controllers. These spikes should appear on either side of the gain spectrum of the erbium-doped fibre, and should indicate that it is feasible to achieve mode locking. The P-controllers are extremely sensitive to movement and need to be moved carefully. Even so, it is very hard to detect these mode-spikes on the oscilloscope, probably because the sampling rate of oscilloscope is not fast enough and these mode-spikes are super-narrow corresponding to maybe one pixel. Another way of detecting mode locking is to look at the two-photon absorption in a silicon detector. The probability for two-photon absorption is very low for CW operation but increases once the laser is showing a tendency to mode lock and becomes very high for a mode locked laser. Unfortunately, we didn't get any closer to mode locking with this measurement technique.

The final call was to use a high-speed InGaAs detector and try to mode-lock the laser in the time domain instead. The detector has a rise time of 70 ps which is sufficient enough to detect mode locking in our configuration, considering that the duration between the pulses should be about τ_r = 19 ns, calculated with equation (3.1). Setting up the InGaAs detector, focusing the output and then by adjusting the P-controllers to increase the amplitude of the noise showing on the oscilloscope we momentarily mode locked the laser. The InGaAs detector was calibrate by using a Ti:Sapphire laser with well known pulse spacing. In Figure 3.7 the pulse train is shown with a separation of ~18.97 ns which corresponds well with the calculated τ_r = 19 ns.

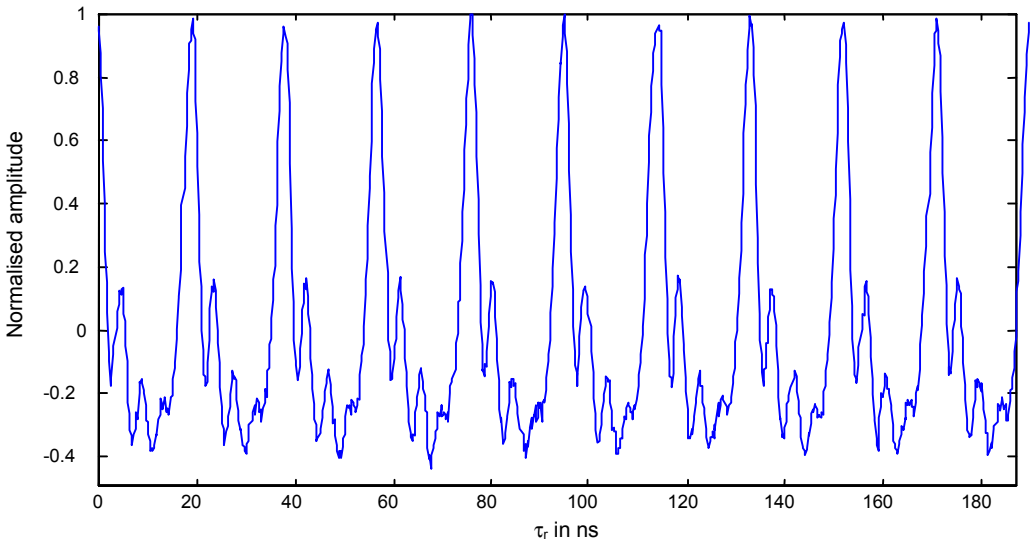

Figure 3.7.

The laser jumps in and out off mode locking randomly, the longest period of time the laser maintained mode locked was for about 1 second. The reason for this might be that the enhanced spectrum that has its origin from SPM becomes too broad in order for the dispersion to balance it. Hence, the spectrum might become too broad to maintain a stable pulse.

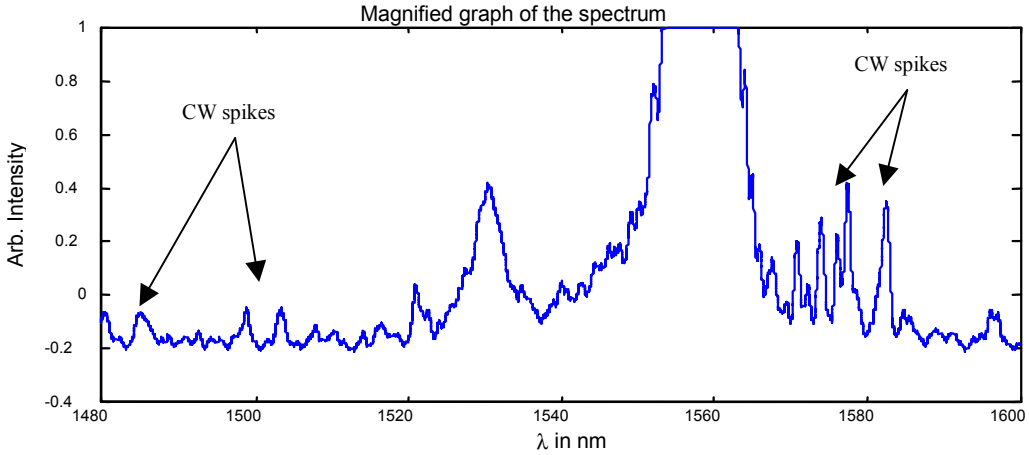

Figure 3.8.

The mode locked spectrum in [17] ranges from 1500 nm to 1600 nm and had a FWHM of ~ 50 nm, which indicates that we are not far from a stable mode locking. Detecting the pulse train with the InGaAs detector in this set up we found that it was similar to what has been shown in Figure 3.7 When trying to find this regime, where the mode locking is momentarily created, it was easier to find it without the BFP. Perhaps the reason for this is that the BFP acts as a filter and when the pulse is generated the newly created frequencies in the wings of the spectrum is coupled out of the cavity. Which in turn means that a lot of power is coupled out of the cavity as well and the induced Kerr effect in the P-controllers has lost its effect. Figure 3.8 is recorded without the BFP. What is usually done when obtaining these mode-spikes in a solid-state laser is to change the dispersion of the cavity to balance the SPM. One way of accomplish this in an all-fibre system is to splice on fibre connectors and use a

patch cord with different lengths of SMF28. SMF28 has negative GVD and can compress a linearly chirped spectrum and in this way get a stable pulse operation of the fibre ring laser. From the first section I can conclude that this is the approach that will give a stable mode-locked pulse. Because of lack of time this could not be done, but the Ultra Fast Optics Group will at a later point conduct further work on this laser.

4 Conclusions

It has been shown that the numerical calculations of the non-linear Schrödinger equation can be used for designing similar all-fibre ring lasers. In order to achieve higher accuracy the Maxwell-Bloch equations must be included, this can be done in the program. Also, the physics behind the laser with its important characteristics has been depicted, i.e., launched pump power and dispersion.

The measurements on the GVD for the different fibres were straightforward and the results could be used in a sufficient way for the construction of the fibre ring laser. The dispersive Fourier transform spectroscopy is a well-known method and has a good accuracy for the measurements done here.

Although the laser did not achieve a stable mode locking during this relative brief project, a compact and an effective laser source was constructed. The maximum CW output from the laser was among the highest reported, 47 mW, and once the ability to change the net dispersion *in situ* with patch cords, this laser will have a stable mode locked pulse.

5 Reference

[1] D.E. Spence, P.N. Kean and W.Sibett, “60 fsec pulse generation by a dispersion-compensated, coupled-cavity, mode-locked Ti:sapphire laser”, Opt. Lett.,Vol.16, pp 42 - 44, Jan.1991.

[2] L.F. Mollenauer and R.H. Stolen, Opt. Lett.,Vol. 9, No. 13, 1984.

[3] K. Tamura, H.A. Haus and E. P. Ippen, Ele. Lett., Vol. 28, No. 24, Nov., 1992.

[4] K. Tamura, E. P. Ippen, H.A. Haus and L.E. Nelson, Opt. Lett.,Vol. 18, No. 13, july, 1993.

[5] Shu Namiki,, E.P. Ippen, H.A. Haus and C.X. Yu, Opt. Soc. Am., Vol. 14, No. 8, Aug, 1997.

[6] G.P. Agrawal, Nonlinear fiber optics, 2nd ed. Chap 2, 6 and 11.

[7] C.Rulliere, Femtosecond Laser Pulses Principles and Experiments, Chap. 1.

[8] J.C. Diels and W. Rudolph, Ultrashort Laser Pulse Phenomena, Chap. 3.

[9] E. Desurvire, J. of lightwave tech.,”Study of the complex atomic susceptibility…”, Vol. 8, No. 10, Oct 1990.

[10] G.P. Agrawal, Phy. Rev A, Vol. 44, No. 11, Dec 1991

[11] V.I. Kruglov, et al.,”Self-similar propagation of high-power…”, Opt. Lett., Vol. 25,No. 24, Dec. 2000.

[12] A.E. Seigman, Lasers, University Science Books, 1986.

[13] L. Råde, B. Westergren, Beta Mathematics Handbook, 2nd edition.

[14] D.A. Flavin et al., Journal of lightwave technology, Vol. 13, No. 7,july 1995.

[15] G.L. Squires, Practical physics, 3rd edition.

[16] K.Tamura et al. Optics letter, Vol. 19, No. 1 /Jan 1, 1994

[17] G.Lenz,et al., All-solid-state femtosecond source at 1.55 microns, Opt. Lett., Vol. 20, No. 11, July 1995

[18] A. Bjarklev, Optical fiber amplifiers: Design and system applications, Chap. 3, Arech House.